EFFICIENCY OPTIMIZATION OF PMSM BASED DRIVE SYSTEM

By

WALEED J. HASSAN

A THESIS

Submitted to
Michigan State University
in partial fulfillment of the requirements
for the degree of

MASTER OF SCIENCE

ELECTRICAL ENGINEERING

2011

ABSTRACT

EFFICIENCY OPTIMIZATION OF PMSM BASED DRIVE SYSTEM

By

WALEED J. HASSAN

The high switching frequency associated with pulse width modulation (PWM) that is commonly utilized in controlling the motion of high performance motor drive systems leads to motor iron losses. In addition to fundamental component, line voltages generated by voltage source inverters or other types of converters include harmonic components. Minimization of the harmonic losses leads to higher motor efficiency. Minimization of the harmonic losses can be accomplished in two stages: first at the design time and the second at the test time. In the first stage, the motor design can be optimized such that it can work in an efficient way for a given range of switching frequencies. In the second stage, the operation of the machine and inverter is optimized such that the total losses of the machine and inverter can be minimized. By measuring the motor harmonics loss for a given switching frequency, it is possible to find analytical model that is suitable for estimating the motor harmonics at all operating points. It is also possible to find the optimum switching frequency, modulation index, and power factor that minimize the motor-inverter total loss.

Since it is difficult or inaccurate to estimate the harmonic losses of machine through analytical approach, most researchers resort to finite element analysis (FEA) instead of analytical solution. The limitation of using finite element software is that it is both time-consuming and difficult to be implemented in real-time control algorithms. For example, if it is required to optimize a design that is constructed and analyzed in FEA software, hours are typically needed to complete such a task.

The proposed work in this thesis is a combination of analytical and numerical methods that are able to calculate the PMSM harmonic losses at any operating point with less execution time and adequate accuracy. Moreover, the motor fundamental losses and the voltage source inverter losses are also modeled such that the inverter-motor efficiency can be tested for different conditions. Numerical simulation of the field oriented control have been conducted and results include current, modulation index, power factor, switching frequency and all the variables in the drive system. Furthermore, Maximum efficiency control strategy has been chosen such that the drive system can work at the most efficient condition at all operation points. The proposed work is presented in the context of drive system that is based permanent magnet synchronous machine (PMSM). However, the proposed method can be extended to induction motor drive system or any motor use SPWM in controlling the inverter output voltage.

Copyright by
WALEED J. HASSAN
2011

I would like to give my deepest appreciation to my parents, who brought me up with their love and encouraged me to pursue advanced degrees. I would like to give my heartfelt appreciation to my wife, who has accompanied me with her love, unlimited patience, understanding and encouragement. Without her support, I would never be able to accomplish this work.

ACKNOWLEDGMENT

First of all, I would like to thank my thesis advisor and mentor Professor Bingsen Wang for his appreciated effort and support throughout my study in ECE and MSU. Thanks to him for spending his valuable time in guiding and encouraging me toward my degree. My thanks extend to my committee members Professor Fang Peng and Professor Joydeep Mitra for their precious comments and advices. Also, I would like to thank all my friends who helped me and wished me good luck in my life.

TABLE OF CONTENTS

LIST OF TABLES

LIST OF FIGURES

Chapter 1

Introduction

Loss modeling and control of high performance motor drive system has been one of attractive research areas since reduced system losses can be translated to lowered energy cost. The primary objective of this thesis is to calculate the motor inverter loss accurately such that the motor drive system can operate at maximum efficiency in all operating conditions. A literature survey has been conducted to include the most up-to-date research results that are focused on modeling and evaluation of different types of losses of permanent magnet synchronous machines (PMSMs).

1.1 Literature Review

The state of the art in the following areas is discussed in this section:

- Motor fundamental losses and efficiency

- Motor harmonic losses

1.1.1 Motor Fundamental Losses and Efficiency

The efficiency and power density of PMSM have been studied by several researchers [1–3]. It has been shown that PMSM features significantly higher efficiency than induction motors when used in adjustable speed drives. Reference [4] provides an analytical method for estimating the fundamental losses of surface mounted PMSM. Several researchers have utilized electrical model of PMSM that includes a parallel resistance that accounts for core losses in high performance applications [5–10]. It can be concluded that both copper and core losses need to be accounted for in the analysis and control of high performance motor drives.

1.1.2 Motor harmonic losses

The iron losses of induction motors, permanent-magnet synchronous motors, and switched reluctance motors have been studied by several researchers [11–17]. Lee and Nam present the loss distribution of three-phase induction motor fed by a PWM inverter both experimentally and by use of variable time-step finite element method (FEM) [11]. The results show that PWM inverters increase the reactive power while decreasing torque. Authors of [12] investigate experimentally the different losses of three-phase induction machines fed by PWM inverter. The test results indicate that increasing the converter switching frequency leads to increased total motor losses, and the loss increase is more pronounced at low speed. Reference [14] estimates the core loss of flux reversal machines (FRM) under four different modes PWM using a 2-D time-stepped voltage source FEM. The result of comparing the losses at the different modes shows that The ON-PWM mode generates higher stator eddy current losses. Toda and Ishida investigate the iron losses of a permanent magnet brushless dc

motor under different stator core lamination sheets material using FEA and various experiments [15]. Sagarduy et. al. introduce experimental results of iron losses in two non oriented electrical steels magnetized by using three-phase voltage source inverter carrier based PWM and three-phase matrix converter space-vector-modulation (SVM) [16]. Their results show that the eddy current loss in the iron material excited by matrix converter is lower than that under PWM excitation. In [17] the authors investigate both experimentally and by FE calculations the iron loss of interior permanent magnet machines driven by PWM inverters. The investigations show that the carrier of PWM generates the highest iron loss component under low speed condition.

Experimental inquiry of the iron loss with different PWM parameters is presented in [18–22]. Authors of [18] study the properties of non-oriented laminations when they are excited by PWM voltage supply. The results show that the variation of PWM voltage supply parameters lead to change the properties of laminations. The effect of PWM switching frequency on the iron loss in soft magnetic material has been investigated in [19]. The experimental results show that the change in the iron losses is not significant with switching frequency higher than 4 kHz. Authors of [20] examine the effect of modulation index on the iron losses of induction motor and wound cores realized with high quality grain oriented magnetic material. The results show that driving the machine with a variable dc link voltage such that the modulation index constant and near unity reduces the iron losses. The eddy-current loss is the dominating loss mechanism according to theoretical research and experiments carried out in the past [23–26].

The theoretical analysis which study the effect of PWM parameters on the iron losses is provided in [27]. The authors have found direct analytical expression for a three-phase trans-

former and dc motor iron loss with PWM parameters. The symmetrical regular sampling rule is used to model PWM output voltage and Fourier series expansion has been employed to extract the harmonics. Also, the authors have assumed that the flux is proportional to the applied voltage. However, the analytical tool used in [27] cannot be applied in analysis of sophisticated systems such as three-phase induction motor variable speed drive system or PMSM variable speed drive system. The inapplicability is due to the following reasons:

- Fourier series provide accurate results only in integer frequency modulating ratios.
- The iron loss caused by carrier waveform fully depends on the phase current and is controlled by the load, speed, depth of modulation and dc bus voltage. Working on the voltage instead of current will give inaccurate results.
- It is not enough to calculate the individual effect of each parameter of PWM on the iron losses. In other words, if it is required to calculate the harmonic losses of variable speed drive system as a whole under different operating conditions.

1.2 Thesis Organization

Chapter 2 provides analytical model of PMSM harmonic losses based on the armature reaction field produced by three-phase current of stator winding. Double Fourier series for naturally sampled sinusoidal PWM (SPWM) has been utilized for evaluation and analysis. Chapter 3 presents analytical-numerical method of loss calculation for three-phase inverter controlled by SPWM. Chapter 4 provides complete dynamic model of PMSM that includes the core loss resistance necessary to calculate the fundamental core loss in steady state. In Chapter 5, a comprehensive field oriented control model for variable speed drive system is

built. The model contains all needed transformation to rotor reference frame and PI controller that are utilized in detailed time-domain simulation. The optimal-efficiency control strategy is implemented in Chapter 6. The results and conclusion are presented in Chapter 7.

1.3 Summary of Contributions

The main contributions of the thesis work are summarized in the following aspects:

- Modeling the harmonics loss of surface mounted PMSM caused by the non sinusoidal stator winding currents.
- Calculating the PMSM harmonics loss using double Fourier analysis of SPWM based on the developed model of the PMSM harmonics loss.
- Modeling the PMSM in dynamic and steady states including the all types of losses (copper, core, mechanical) and characterizing the efficiency at any operating condition.
- Calculating the losses of the voltage source inverter by analytical model supplied by numerically generated parameters (modulation index, current, displacement angle),such that the dynamic behaviour of the losses can be tested in all conditions.
- Constructing a complete SIMULINK model that includes what have been mentioned above in field oriented control system and designing all needed currents and speed controllers.
- Implementation of the maximum efficiency control strategy, such that the system can operate under optimal fundamental efficiency at all load, and speed conditions.

Chapter 2

PMSM Harmonics Loss Modeling and Evaluation

The core losses in the machine consist of two components, i.e., hysteresis and eddy current losses. Both types of core loss are due to time variation of the flux density in the core. The hysteresis loss is the result of the inherent $B-H$ material characteristics and is proportional to the product of frequency and flux density with the flux density raised to a power β, which is generally termed as Steinmetz constant. The value of β ranges from 1.5 to 2.5 and is dependent on peak operating flux density and material characteristics [28]. In this thesis work the value of Steinmetz constant is assumed to be 2.

As the flux linkage changes with time, an electromagnetic motive force (EMF) is induced in core. The induced EMF generates a current in the core depending on the electric conductivity of the core, which will in turn result in losses that are termed the eddy current losses. The eddy current losses are proportional to the square of the induced EMF and hence proportional to square of the product of frequency and flux density. The complete expression

for core losses in $\left[\mathrm{Wm}^{-3}\right]$ is:

$$P_{cd} = P_{ed} + P_{hd} = K_e \sum_{n=1}^{\infty} (n\omega_r)^2 B_{p,n}^2 + K_h \sum_{n=1}^{\infty} n\omega_r B_{p,n}^{\beta} \tag{2.1}$$

where K_e is the eddy loss proportionality constant that accounts for volume to weight conversion and all other particular constants are associated with magnetic materials; K_h is the hysteresis loss density; $B_{p,n}$ is the peak flux density of the nth-order and fundamental angular frequency of applied voltage is ω_r. In Equation (2.1) when $n = 1$, the core loss equation evaluates the losses caused by the fundamental flux density. However, for $n = 2 \rightarrow \infty$, Equation (2.1) evaluates the harmonics loss associated with the harmonic component of the flux. Evaluation of the fundamental loss of PMSM analytically and in FEA software have been extensively covered in the literature over the last years. However, the harmonic loss caused by PWM has not been studied in depth, which is particularly true for induction and permanent magnet synchronous machines . In the next section an accurate analytical harmonics loss model based on flux equation by Zhu in 1993 will be introduced [29].

2.1 Harmonics Iron Losses of Surface Mounted PMSM

In this section analytical model for motor harmonic loss is developed based on the work published in [29] where the armature reaction field produced by the stator winding is predicted. The armature reaction field produced by a single-phase stator winding is:

$$B(\alpha, r, t) = \mu_{\circ} \frac{2W}{\pi} \frac{i}{\delta} \sum_{v} \frac{1}{v} K_{sov} K_{dpv} F_v(r) \cos(v\alpha) \tag{2.2}$$

where $\alpha = 0$ refers to the axis of the phase winding; W is the number of series turns per phase; and $K_{dpv} = K_{dv}K_{pv}$, with K_{dv} being the winding distribution factor and K_{pv} being the pitch factor. $F_v(r)$ is a function dependant on the radius and harmonics order, and given by:

$$f_v(r) = \delta\frac{v}{r}\left(\frac{r}{R_{si}}\right)^v \frac{1+\left(\frac{R_{si}}{r}\right)^{2v}}{1-\left(\frac{R_r}{R_{si}}\right)^{2v}} \tag{2.3}$$

where R_r is rotor radius; $\delta = g + h_m$ is the effective airgap length with g being the air gap and h_m being radial magnet thickness. When the number of slots per pole per phase is an integer, the distribution factor K_{dv} is given by:

$$K_{dv} = \frac{sin\left(q\frac{v\pi}{Qs}\right)}{q\sin\left(\frac{v\pi}{Qs}\right)} \tag{2.4}$$

where q is the number of stator slots per pole per phase, and given by:

$$q = \frac{Q_s}{2P_p m} \tag{2.5}$$

where Q_s is the total number of slots; m is the number of phases; and P_p is the number of pole pairs. The winding pitch factor K_{pv} is given by:

$$K_{pv} = \sin\left(\frac{v\alpha_y}{2}\right) \tag{2.6}$$

where α_y is the winding pitch. The values of the summation index v is given by:

$$
\begin{aligned}
v &= P_p\left(6c - \{\pm u\}\right) \\
&= P_p\left(6\left\{0,1,2,...,\right\} - \{1,5,7,...,\}\right) + P_p\left(6\left\{0,-1,-2,...,\right\} - \{-1,-5,-7,...,\}\right) \\
u &= 1,5,7,11,13,17,19,23,25,29,35,37 \\
c &= 0 \pm 1 \pm 2 \pm 3,...
\end{aligned}
$$

The slot opening factor K_{sov} is defined as:

$$K_{sov} = \frac{\sin\left(\frac{vb_\circ}{2R_{si}}\right)}{v\left(\frac{b_\circ}{2R_{si}}\right)} \tag{2.7}$$

where $b_\circ$ is the slot-opening width; R_{si} is the stator inner radius. Clearly if the slot-opening $b_\circ$ is very small, i.e., $b_\circ \to 0.$, then the slot-opening factor approaches unity, i.e, $K_{sov} \to 1$. The phase winding currents of PMSM controlled by SPWM contain significant harmonics and can be expressed by Fourier series as:

$$i_a = \sum_n I_n \sin\left[n\left(P_p\omega_m t\right) + \theta_n\right] \tag{2.8}$$

$$i_b = \sum_n I_n \sin\left[n\left(P_p\omega_m t - \frac{2\pi}{3}\right) + \theta_n\right] \tag{2.9}$$

$$i_c = \sum_n I_n \sin\left[n\left(P_p\omega_m t - \frac{4\pi}{3}\right) + \theta_n\right] \tag{2.10}$$

where $\theta = P_p\omega_m t$, ω_m is the rotor mechanical angular frequency in [rad s^{-1}]; and θ_n is the harmonic phase angle. Hence the field produced by a three-phase winding can be deduced

from (2.2),(2.8),(2,9) and (2,10) as :

$$B_{3\phi}(\alpha, r, t) = B_a(\alpha, r, t) + B_b(\alpha, r, t) + B_c(\alpha, r, t) \tag{2.11}$$

$$= \left\{ \begin{array}{c} \mu_\circ \frac{2W}{\pi\delta} \sum_v \frac{1}{v} K_{sov} K_{dpv} F_v(r) \ldots \\ \left\{ i_a \cos(v\alpha) + i_b \cos\left(v\left(\alpha - \frac{2\pi}{3P_p}\right)\right) + i_c \cos\left(v\left(\alpha - \frac{4\pi}{3P_p}\right)\right) \right\} \end{array} \right\} \tag{2.12}$$

$$= \{\mu_\circ \frac{2W}{\pi\delta} \sum_n I_n \sum_v \frac{1}{v} K_{sov} K_{dpv} F_v(r)\} \sin(n\omega_r t + v\alpha + \theta_n) \tag{2.13}$$

where $\omega_r = P_p \omega_m$ is the electrical rotor angular speed in $[\mathrm{rad\,s^{-1}}]$; B_p is the maximum amplitude of armature reaction flux density determined by:

$$B_p = \mu_\circ \frac{2W}{\pi\delta} \sum_n I_n \sum_v \frac{1}{v} K_{sov} K_{dpv} F_v(r) \tag{2.14}$$

2.1.1 Eddy Current Loss

Once the maximum amplitude of the flux density has been defined, which results from the armature space vector current, the procedure of finding accurate model for core loss is shown in the following approximate expression.

$$P_{ed} \propto \sum_n \left(n f_r B_{p,n}\right)^2 \propto \sum_n \left(n\omega_r B_{p,n}\right)^2 \tag{2.15}$$

The proportionality expressed in (2.15) represents the first principle in development of the eddy current loss model, which can be translated to

$$P_{ed} = K_e \sum_n (n\omega_r)^2 B_{p,n}^2 \tag{2.16}$$

By plugging equation (2.14) in (2.16) and defining the volume in which the loss are evaluated, the expression to evaluate eddy core loss as will be reached

$$\begin{aligned} P_e &= (\rho_i V)\, P_{ed} \\ &= (\rho_i V)\, K_e \sum_n (n\omega_r)^2 B_{p,n}^2 \\ &= (\rho_i V)\, K_e \sum_n (n\omega_r)^2 \left(\mu_\circ \frac{2W}{\pi\delta} \sum_n I_n \sum_v \frac{1}{v} K_{sov} K_{dpv} F_v(r) \right)^2 \\ &= \left((\rho_i V)\, K_e \left(\mu_\circ \frac{2W}{\pi\delta} \right)^2 \left(\sum_v \frac{1}{v} K_{sov} K_{dpv} F_v(r) \right)^2 \right) \sum_n (n\omega_r)^2 I_n^2 \\ &= K_{em} \sum_{n=1}^{\infty} (n\omega_r)^2 I_n^2 \end{aligned} \tag{2.17}$$

where ρ_i is the mass density of the steel core material in [kg m^{-3}]; V is the steel core volume in [m^3]; and their product gives the weight of the core material in [kg]. K_{em} is defined as:

$$K_{em} = (\rho_i V)\, K_e \left(\mu_\circ \frac{2W}{\pi\delta} \right)^2 \left(\sum_v \frac{1}{v} K_{sov} K_{dpv} F_v(r) \right)^2 \tag{2.18}$$

2.1.2 Hysteresis Loss

Following the same procedure as the last section, an expression for hysteresis loss can be reached as presented in equations (2.20) and (2.21):

$$P_{hd} \propto \sum_n n f_r B_{p,n}^2 \propto \sum_n n\omega_r B_{p,n}^2 \tag{2.19}$$

$$P_{hd} = K_h \sum_n n\omega_r B_{p,n}^2 \tag{2.20}$$

$$
\begin{aligned}
P_h &= (\rho_i V)\, P_{hd} \\
&= (\rho_i V)\, K_h \sum_n n\omega_r B_{p,n}^2 \\
&= (\rho_i V)\, K_h \sum_n n\omega_r \left(\mu_\circ \frac{2W}{\pi\delta} \sum_n I_n \sum_v \frac{1}{v} K_{sov} K_{dpv} F_v\,(r) \right)^2 \\
&= \left((\rho_i V)\, K_h \left(\mu_\circ \frac{2W}{\pi\delta} \right)^2 \left(\sum_v \frac{1}{v} K_{sov} K_{dpv} F_v\,(r) \right)^2 \right) \sum_n n\omega_r I_n^2 \\
&= K_{hm} \sum_{n=1}^{\infty} n\omega_r I_n^2
\end{aligned}
\tag{2.21}
$$

The coefficient K_{hm} is defined as:

$$
K_{hm} = (\rho_i V)\, K_h \left(\mu_\circ \frac{2W}{\pi\delta} \right)^2 \left(\sum_v \frac{1}{v} K_{sov} K_{dpv} F_v\,(r) \right)^2 \tag{2.22}
$$

The final expression for the core loss in [W] is given by:

$$
\begin{aligned}
P_c &= P_e + P_h \\
&= K_{em} \sum_{n=1}^{\infty} (n\omega_r)^2 I_n^2 + K_{hm} \sum_{n=1}^{\infty} n\omega_r I_n^2
\end{aligned}
\tag{2.23}
$$

Close examination of K_{em} and K_{eh} shows that they are constant for a given machine design since they solely depend on the machine dimensions. On the other hand, the core harmonic loss can be expressed as:

$$
\begin{aligned}
P_{c,h} &= P_{e,h} + P_{h,h} \\
&= K_{em} \sum_{n=2}^{\infty} (n\omega_r)^2 I_n^2 + K_{hm} \sum_{n=2}^{\infty} n\omega_r I_n^2
\end{aligned}
\tag{2.24}
$$

It is clear that the motor harmonics loss can can be fully evaluated if the amplitudes of current harmonics determined. In the next section the analytical relationship between the current harmonics sum and the harmonics content of SPWM line voltage will be presented.

2.2 SPWM Harmonics Analysis

For three-phase inverter with two-level phase legs, a balanced set of three-phase line-line output voltages is obtained if the references are displaced by 120°. Under these conditions, the line to line voltages are given for naturally sampled PWM by [30]:

$$\mathrm{v}_{l-l}\left(\omega_{\circ},\omega_{c}\right)=\left\{\begin{array}{l}\left[\sqrt{3}\,\frac{V_{dc}}{2}M\right]\cos(\omega_{\circ}t+\frac{\pi}{6})+\ldots\\ \\ \left[\frac{4V_{dc}}{\pi}\sum\limits_{m=1}^{\infty}\sum\limits_{n=-\infty}^{\infty}\frac{1}{m}J_{n}\left(m\frac{\pi}{2}M\right)\sin\left(\left[m+n\right]\frac{\pi}{2}\right)\sin\left(n\frac{\pi}{3}\right)\right]\ldots\\ \\ \cos\left(m\omega_{c}t+n\left[\omega_{\circ}t-\frac{\pi}{3}\right]+\frac{\pi}{2}\right)\end{array}\right\} \tag{2.25}$$

Equation (2.25) clearly indicates that the triplen sideband harmonics of the carrier are cancelled because the term $\sin\left(n\frac{\pi}{3}\right)$ will be zero when $n=3,6,9,....$ Hence the major significant sideband harmonics that are left will be: $f_h=f_s\pm 2f_{\circ}, f_s\pm 4f_{\circ}, 2f_s\pm 5f_{\circ}$. The sideband cancellation is not caused by any specific carrier ratio requirement. Therefore, there is no identifiable benefit with regard to harmonic performance by maintaining an odd carried/fundamental ratio [30]. Figure 2.1 shows the harmonic components of the line-line voltage generated by a three-phase inverter switched by double-edge naturally sampled PWM. The predicted significant sideband harmonics in the first and second carrier group can be clearly identified. The surface mounted PMSM can be analyzed as a single phase circuit that consists of series impedance and back emf since the reactances on the d-axis and the q-axis are identical. At harmonic frequencies 3,6,9 stator resistance and back emf are neglected so that the motor modeled as synchronous inductance only. The motor phase

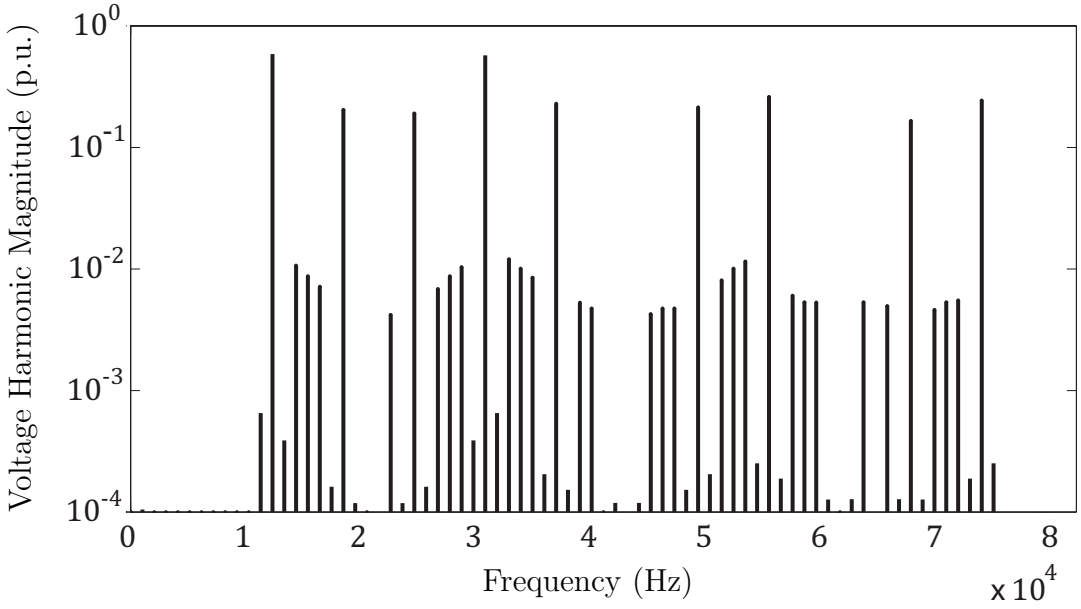

Figure 2.1: Theoretical harmonic spectra for a three-phase inverter modulated by naturally sampled PWM.

current can be determined by the phase voltage and the synchronous inductance of the stator winding. With the assumption of star connection of PMSM, the phase current is given by:

$$\begin{aligned} I(\omega)_{\omega \neq \omega_\circ} &= \frac{v_{ph}(\omega)}{\omega L_s} \\ &= \frac{1}{\sqrt{3}}\left(\frac{1}{L_s}\right)\frac{v_{l-l}(\omega)}{\omega} \\ &= K\frac{v_{l-l}(\omega)}{\omega} \end{aligned} \tag{2.26}$$

where v_{ph} is the phase-to-neutral voltage; ω is angular harmonic frequency; L_s is motor synchronous inductance. K is defined as:

$$K = \frac{1}{\sqrt{3}}\left(\frac{1}{L_s}\right) \tag{2.27}$$

Plugging equation (2.25) in equation(2.26) yields:

$$\left|I_{m,n}(\omega)\right|_{\omega\neq\omega_\circ} = \left|K\left[\frac{4V_{dc}}{\pi}\sum_{m=1}^{\infty}\sum_{n=-\infty}^{\infty}\frac{1}{\omega_{m,n}}\frac{1}{m}J_n\left(m\tfrac{\pi}{2}M\right)\sin\left(\left[m+n\right]\tfrac{\pi}{2}\right)\sin n\tfrac{\pi}{3}\right]\right| \quad (2.28)$$

Alternatively, Equation (2.28) can be expressed as a function of harmonic frequency:

$$\left|I_{m,n}(f)\right|_{f\neq f_\circ} = \left|\left(\frac{1}{2\pi\sqrt{3}L_s}\right)\left[\frac{4V_{dc}}{\pi}\sum_{m=1}^{\infty}\sum_{n=-\infty}^{\infty}\frac{1}{f_{m,n}}\frac{1}{m}J_n\left(m\tfrac{\pi}{2}M\right)\sin\left(\left[m+n\right]\tfrac{\pi}{2}\right)\sin n\tfrac{\pi}{3}\right]\right| \quad (2.29)$$

Let $\omega_{m,n}$ be defined as:

$$\begin{aligned}\omega_{m,n} &= 2\pi f_{m,n}\\ &= 2\pi\left(mf_{sw}+nf_\circ\right)\end{aligned} \quad (2.30)$$

where f_{sw} is the inverter switching frequency and $f_\circ$ is the motor fundamental frequency.

The motor harmonics loss discussed in the last section is incomplete since the current harmonics sum was not defined yet. After the current harmonics amplitudes in determined by (2.28) or (2.29), the motor harmonic core loss is readily determined as the following:

$$\begin{aligned}P_{c,h} &= P_{e,h}+P_{h,h}\\ &= K_{em}\sum_{m=1}^{\infty}\sum_{n=-\infty}^{\infty}\left(\omega_{m,n}\left|I_{m,n}\right|_{f\neq f_\circ}\right)^2 + K_{hm}\sum_{m=1}^{\infty}\sum_{n=-\infty}^{\infty}\omega_{m,n}\left(\left|I_{m,n}\right|_{f\neq f_\circ}\right)^2\end{aligned} \quad (2.31)$$

Chapter 3

Loss Calculation and Analysis of Voltage Source Inverter

The research effort in this thesis is to optimize not only the PMSM efficiency, but also the drive system as a whole after the estimation of voltage source inverter loss has been studied. The majority of harmonic losses of the motor, which is caused by PWM carrier frequency, can be minimized by increasing the inverter switching frequency. Nonetheless, the inverter switching loss will concurrently increase, as detailed in the subsequent section. Therefore, for achieving global optimization of the system, one needs to define the value of the optimal frequency that minimizes the motor harmonic loss and inverter losses together. The aim of this chapter is to provide analytical model for the calculation of power losses in IGBT-based voltage source inverter used in PMSM drive system. The inverter parameters of the semiconductor switches in the inverter have been extracted from the data sheets of FAIRCHILD, RURG5060 and HTGT30N60A4 modules.

A number of different methods have been proposed to estimate the losses of voltage source

inverters. The first is based on the complete numerical simulation of the circuit by specific simulation programs with integrated or parallel-running losses calculations. The second is to calculate the electrical behaviour of the circuit based on analytical behaviour model [31]. For accurate estimation of the losses during the transient time and all operating conditions, a hybrid model has been developed. In this model, the operating conditions that are resulted from the numerical simulation of the motor drive system are utilized in the analytical model.

The losses in a power-switching device consist of conduction losses, switching losses and off-state blocking loss. The off-state blocking loss is negligible compared to other two types of loss, and is given by the product of the blocking voltage and the leakage current. Switching losses and conduction losses will be analyzed in detail in the following sections.

3.1 Switching Losses of three phase Voltage Source Inverter

For the subsequent calculations a linear loss model for power semiconductors devices is assumed. Switching loss energy E_s will be linearly scaled as the following:

$$E_s = E_{sr} \cdot \frac{V}{V_r} \cdot \frac{I}{I_r} \tag{3.1}$$

where E_{sr} is the rated switching loss energy that is typically given in the device data sheet for reference commutation voltage V_r and reference current I_r while V and I represent the actual commutation voltage and current respectively. The rated switching energy can be defined as the summation of on, off states of each power semiconductor device. For one pair

of IGBT and freewheeling diode, E_{sr} is given by

$$E_{sr} = E_{on,I} + E_{off,I} + E_{off,D} \tag{3.2}$$

where $E_{on,I}$ and $E_{off,I}$ are the turn-on and turn-off energies of the IGBT, respectively; $E_{off,D}$ is the turn-off energy of the power diode due to reverse recovery current. The result of plugging (3.2) in (3.1) E_s is:

$$E_s = \left(E_{on,I} + E_{off,I} + E_{off,D}\right) \cdot \frac{V}{V_r} \cdot \frac{I}{I_r} \tag{3.3}$$

The power loss P_{sr} is related to the energy loss E_{sr} as by

$$E_{sr} = P_{sr} \cdot T \tag{3.4}$$

where T is the switching period. The equation for the switching loss P_{ls} of a VSI with sinusoidal ac line current and with IGBT switching devices is given by:

$$P_{ls} = \frac{6}{\pi} \cdot f_s \cdot (E_{on,I} + E_{off,I} + E_{off,D}) \cdot \frac{V_{dc}}{V_r} \cdot \frac{I_L}{I_r} \tag{3.5}$$

where f_s is the VSI switching frequency; V_{dc} is the dc link voltage and I_L is the peak value of the ac line current that is assumed sinusoidal.

3.2 Conduction Losses of VSI

In contrast to the switching losses, the conduction losses are directly depending on the modulation function [31]. In [32–35] formulas for reckoning the conduction losses depending on the modulation function are presented. Reference [36] provides extensive information on definition of a certain modulation function by the distribution of the duty cycles for the two different zero vectors. With the knowledge of the relevant modulation function the conduction losses $P_{lc,I}$ of a single semiconductor IGBT are expressed by equation:

$$P_{lc,I} = \frac{V_{CE,0}}{2\pi} \cdot I_L \int_0^{\pi} \sin(\omega t) \cdot \frac{1 + M(t)}{2} \cdot d\omega t + \frac{r_{CE,0}}{2\pi} \cdot I_L^2 \int_0^{\pi} \sin^2(\omega t) \cdot \frac{1 + M(t)}{2} \cdot d\omega t \quad (3.6)$$

Likewise the conduction loss that is associated with each diode $P_{lc,D}$ can be written as:

$$P_{lc,D} = \frac{V_{F,0}}{2\pi} \cdot I_L \int_0^{\pi} \sin(\omega t) \cdot \frac{1 - M(t)}{2} \cdot d\omega t + \frac{r_{F,0}}{2\pi} \cdot I_L^2 \int_0^{\pi} \sin^2(\omega t) \cdot \frac{1 - M(t)}{2} \cdot d\omega t \quad (3.7)$$

The sum of the total conduction losses P_{lc} for all twelve semiconductor devices is determined by

$$P_{lc} = 6 \cdot \left(P_{lc,I} + P_{lc,D} \right) \quad (3.8)$$

For the carrier based PWM method equations (3.6) and (3.7) turn into expressions (3.9) and (3.10) [1].

$$P_{lc,I} = \frac{V_{CE,0}}{2\pi} \cdot I_L \left(1 + \frac{M \cdot \pi}{4} \cdot \cos(\phi) \right) + \frac{r_{CE,0}}{2\pi} \cdot \left(\frac{\pi}{4} + M \left(\frac{2}{3} \cdot cos(\phi) \right) \right) \quad (3.9)$$

$$P_{lc,D} = \frac{V_{F,0}}{2\pi} \cdot I_L \left(1 - \frac{M \cdot \pi}{4} \cdot \cos(\phi) \right) + \frac{r_{CE,0}}{2\pi} \cdot \left(\frac{\pi}{4} - M \left(\frac{2}{3} \cdot cos(\phi) \right) \right) \quad (3.10)$$

where M is the modulation index and ϕ is the displacement angle between the fundamental of modulation function and the load current. The total inverter losses at different operation points will be analyzed in the next section.

3.3 Total Losses of VSI

The total losses of the VSI that is realized with practical semiconductor devices have been evaluated based on he parameters used in the numerical simulation are listed in Table 3.1. A plot of the switching loss for a range of switching frequencies is shown in Figure 3.1. It is

Table 3.1: Parameters of the semiconductor devices of the VSI.

Power Devices	Parameters			
IGBT	$I_{ref}\,(A)$	50	$V_{ref}\,(V)$	600
	$E_{on,I}\,(mJ)$	0.6	$E_{off,I}\,(mJ)$	0.966
	$V_{CE,0}\,(V)$	1.6	$r_{CE,0}\,(m\omega)$	15
Diode	$r_{F,0}\,(m\omega)$	8	$V_{F,0}\,(V)$	1.6
	$E_{off,D}\,(mJ)$	0.7		

clear that the switching loss is proportional to switching frequency and maintains constant for a given load current and switching frequency. With respect to conduction losses, the loss depends on load displacement angle, modulation index and load current. Figure 3.2 illustrates the variations of the conduction losses with the load displacement angle under different loading conditions. The plot of conduction loss equation shows that the loss is maximized when the displacement angle is zero and decreases as the displacement angle increases or decreases from zero. In field oriented control of variable speed drive system, for a given speed command the controller will assign voltage proportional to that speed by means of modulation action. However, increasing the motor speed requires higher line to line voltage and causes the motor to draw higher current for constant load torque. In other

words, increasing the motor speed will increase the inverter losses since the current and modulation index will be higher.

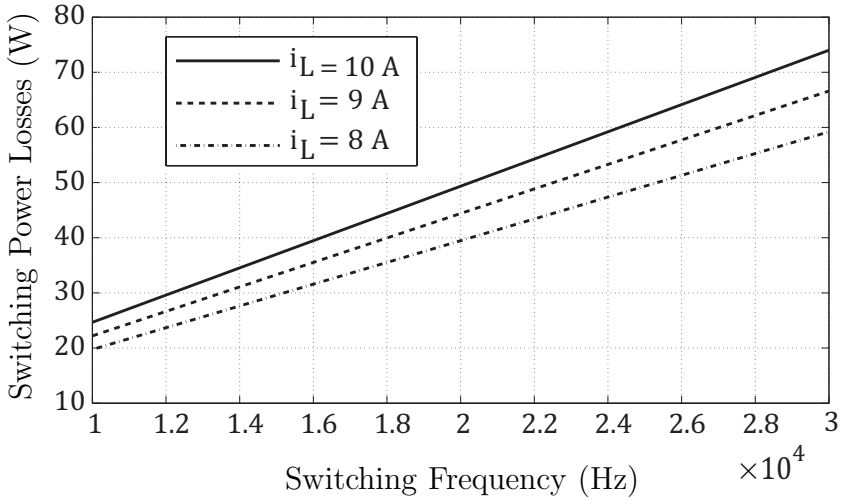

Figure 3.1: Switching losses of VSI at different load currents.

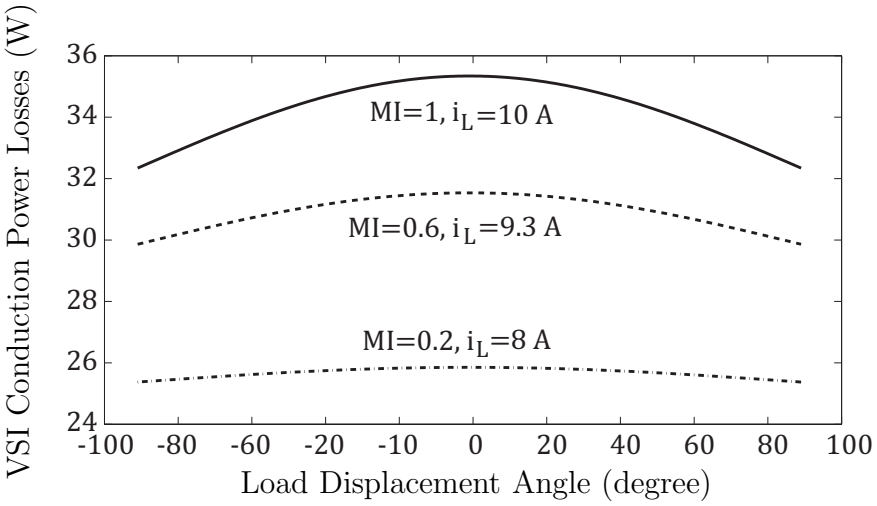

Figure 3.2: Conduction losses of VSI at different modulation indices.

Chapter 4

PMSM Modeling

The use of PMSM has rapidly increased in recent years, especially for high performance applications such as traction, automobiles, robotics and aerospace technology. The PMSM has a sinusoidal back emf and requires sinusoidal stator currents to produce smooth torque. The PMSM is very similar to the standard wound rotor synchronous machine except that the PMSM has no damper windings and its field excitation is provided by permanent magnets instead of a field winding. Hence the *dq*-model of the PMSM can be derived from the well-known model of the synchronous machine with the equations of the damper windings and field current dynamics removed [37]. The transformation of the synchronous machine equations from the abc phase variables to the dq variables forces all sinusoidally varying inductances in the abc frame to become constant in the dq frame.

For the purpose of evaluation of the motor performance in steady state and transient, the model in Figure 4.1 is used. The model in Figure 4.2 is used to calculate motor efficiency, currents and other parameters during steady state operation. The cross saturation model, which is used in controller design, is the most accurate model. In this model q-axis and d-axis

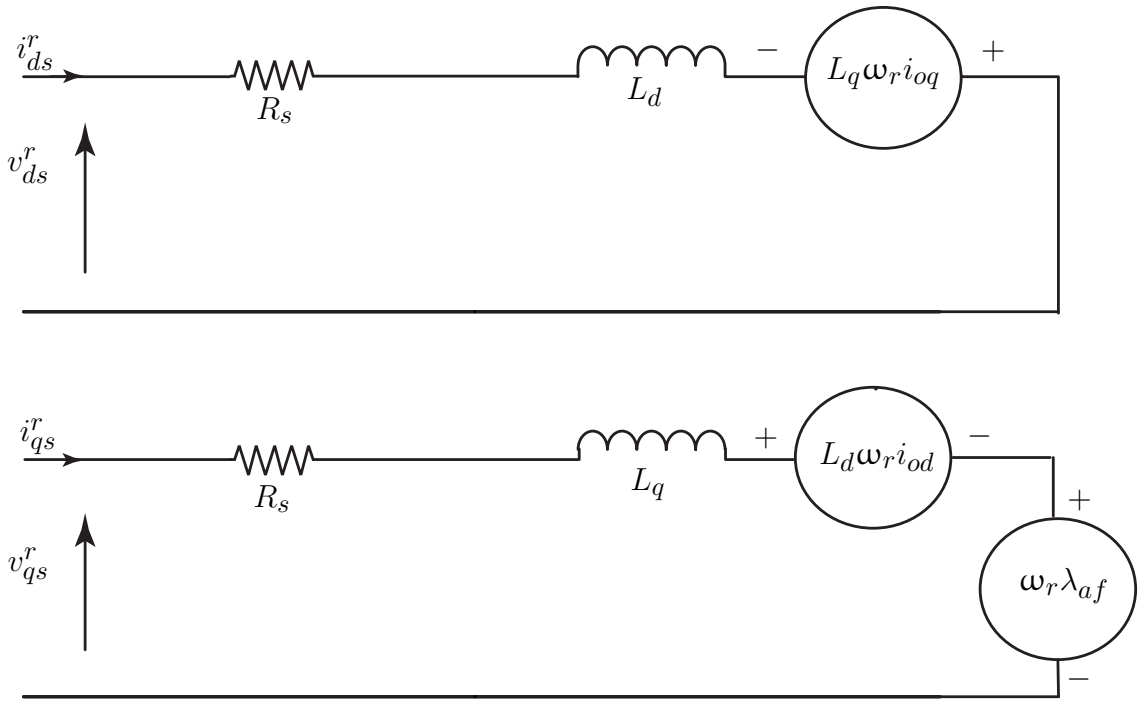

Figure 4.1: Dynamic equivalent circuits of PMSM.

inductances are functions of i_d and i_q as a result of saturation. A lookup table is typically needed to store the measured L_d and L_q corresponding to different i_d and i_q combinations. This model is often used in normalsize size machines in which the iron material more tends to saturate than big size machines.

To evaluate the motor efficiency as a part of a high performance vector controlled servo drive numerically in transient, steady state and in all operating points, the selected model is the dynamic model that includes the core loss resistance as shown in Figure 4.3. The PMSM dynamic model can be divided into two subsystems: electrical system and mechanical system. The details of the complete PMSM model are presented in the next sections.

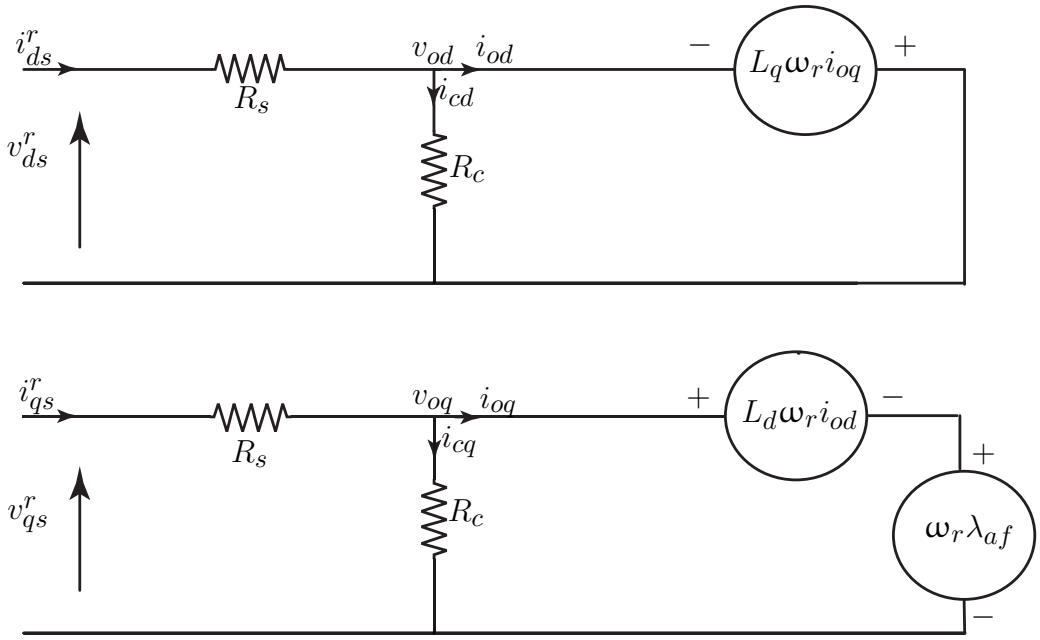

Figure 4.2: Steady state equivalent circuits of PMSM include core loss resistance.

4.1 Electrical System

The electrical system is represented by the electrical equations of the motor that are organized in a way such that the input currents of the model are functions of the input voltages. The selected model is shown in Figure 4.3, where v^r_{qs} and v^r_{ds} are stator voltages on the quadrature and direct axes, respectively. The superscript r refers to rotor reference frame . R_s is the stator winding resistance. R_c is the core loss resistance. i^r_{qs} and i^r_{ds} are motor stator currents on the quadrature and direct axes, respectively. λ_{af} is field flux linkages due to rotor magnets. ω_r is electrical rotor speed in [rad s^{-1}]. The subscript o in the remaining v and i in the circuits refers to output voltages and currents.

To build the dynamic model of the motor, the equations of the motor have to be properly organized such that they can be implemented in SIMULINK model. The first step of developing the model is to rearrange equation (4.1) into the form of equations (4.2) and

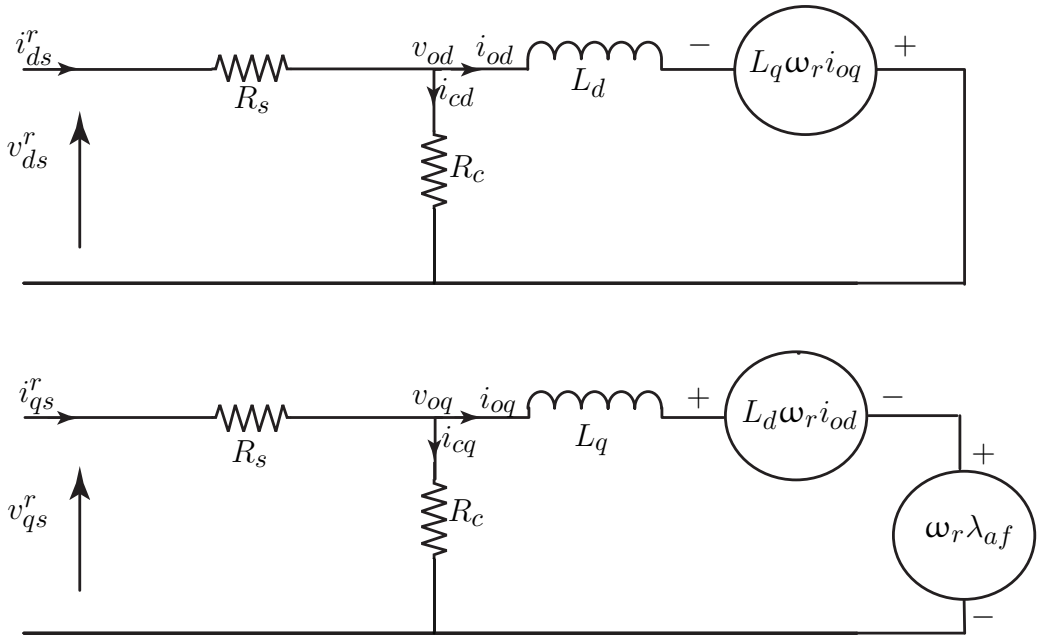

Figure 4.3: Dynamic equivalent circuit of PMSM that includes core resistance.

(4.3) :

$$\begin{bmatrix} v^r_{ds} \\ v^r_{qs} \end{bmatrix} = R_s \begin{bmatrix} i_{od} \\ i_{oq} \end{bmatrix} + \left(\frac{R_c + R_s}{R_c} \right) \begin{bmatrix} v_{od} \\ v_{oq} \end{bmatrix} \tag{4.1}$$

$$v_{od} = \left(\frac{R_c}{R_c + R_s} \right) \left(v^r_{ds} - R_s \, i_{od} \right) \tag{4.2}$$

$$v_{oq} = \left(\frac{R_c}{R_c + R_s} \right) \left(v^r_{qs} - R_s \, i_{oq} \right) \tag{4.3}$$

In equations (4.2) and (4.3), the output voltages are functions of the stator output currents and voltages. The dynamic part of the circuit indicates that the output voltages are functions of the output currents and the rotor speed, which is mathematically represented by:

$$\begin{bmatrix} v_{od} \\ v_{oq} \end{bmatrix} = \begin{bmatrix} L_d \, p & -L_q \, \omega_r \\ L_d \, \omega_r & L_q \, p \end{bmatrix} \begin{bmatrix} i_{od} \\ i_{oq} \end{bmatrix} + \begin{bmatrix} 0 \\ \omega_r \, \lambda_{af} \end{bmatrix} \tag{4.4}$$

where p denotes $\frac{d}{dt}(\ )$. Rearranging of equation (4.4) leads to equations (4.5) and (4.6):

$$i_{od} = \frac{1}{L_d} \left[\int \left(v_{od} + L_q \, \omega_r \, i_{oq} \right) \, dt \right] \tag{4.5}$$

$$i_{oq} = \frac{1}{L_q} \left[\int \left(v_{oq} - L_d \, \omega_r \, i_{od} - \omega_r \, \lambda_{af} \right) \, dt \right] \tag{4.6}$$

It is evident that the output currents are functions of the output voltages, the coupled output current of the other axis, and rotor speed.

The next step is to calculate the currents of the core loss resistance i_{cd} and i_{cq}. They are simply the ratio of output voltage to core loss resistance in each circuit. Since the core loss resistance is used to calculate the core loss in steady state, the dynamic part of the output voltage is neglected. In other words, the voltages due to rate of change in L_d and L_q during the transient are neglected. Equations (4.7) and (4.8) give i_{cd} and i_{cq} as functions of the output currents and rotor speed:

$$i_{cd} = - \left(\frac{L_q}{R_c} \right) \omega_r \, i_{oq} \tag{4.7}$$

$$i_{cq} = \frac{1}{R_c} \left(\lambda_{af} + L_d \, i_{od} \right) \omega_r \tag{4.8}$$

The last step is to calculate the total rotor currents as:

$$i^r_{ds} = i_{od} + i_{cd} \tag{4.9}$$

$$i^r_{qs} = i_{oq} + i_{cq} \tag{4.10}$$

It is worth mentioning that almost all of motor dynamic electrical equations need the motor electrical speed as an input parameter. The motor electrical speed is proportional to its mechanical speed that is derived from the mechanical system. The next section details modeling of the motor speed.

4.2 Mechanical System

The modeling of the motor electrical speed begins at the equation of the electromagnetic torque generated by the PMSM,

$$T_e = \frac{3}{2}\frac{P}{2}\left[\lambda_{af}\, i_{oq} + \left(L_d - L_q\right) i_{od}\, i_{oq}\right] \tag{4.11}$$

where P is the number of poles. Equation (4.11) generally represents the electromagnetic torque generated in the two types of PMSM: interior PMSM and surface mounted PMSM. Surface mounted PMSM can be considered as a special case in which L_d equals L_q. Hence, the reluctance torque of the electromagnetic torque equals zero.

In order for the motor to operate at a given speed, the electromagnetic torque needs to overcome all torque components in the opposite direction, which include load torque, friction torque, and the torque that results from the combined rotor and load moment of inertia. The torque equation is expressed by:

$$T_e = J\frac{d\omega_m}{dt} + T_l + B\,\omega_m \tag{4.12}$$

where J is moment of inertia of the load and machine rotor combined in [kg m^2]. ω_m is rotor mechanical speed in [rad s^{-1}]. T_l is load torque in [N m]. B is friction coefficient of the

load and the machine in [N m rad^{-1}s]. Rearranging of equation (4.12) gives the mechanical speed:

$$\omega_m = \frac{1}{J}\left[\int (T_e - T_l - B\,\omega_m)\,dt\right] \tag{4.13}$$

Finally, the electrical rotor speed is related to mechanical rotor speed by the number of pole pairs:

$$\omega_r = \frac{P}{2}\omega_m \tag{4.14}$$

As another note, the model inputs and outputs quantities are in rotor reference frame. It is necessary to perform the transformations between abc and dq such that the model supplied by the input voltage in stationary reference frame and output the phase currents in stationary reference frame too. The details of necessary transformations are given in the next section.

4.3 Transformations

The block diagram of PMSM in Figure 4.4 shows the necessary transformations. There are two transformations. The first is called three to two transformation, which is mathematically represented by equation (4.15):

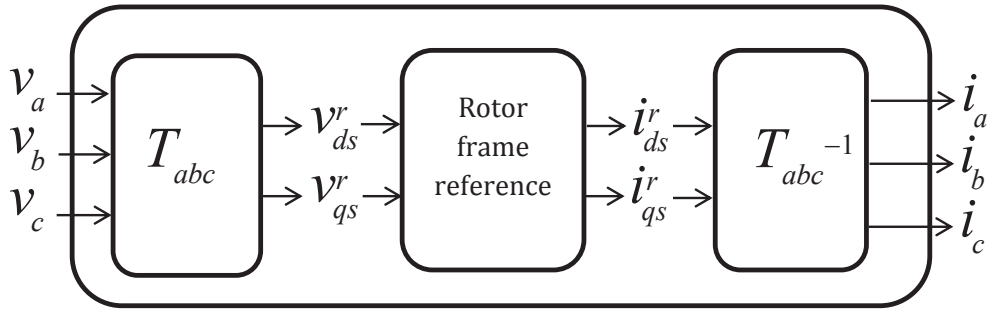

Figure 4.4: Simple schematic model of PMSM.

$$T_{abc} = \begin{bmatrix} \cos\theta_r & \cos\left(\theta_r - \frac{2\pi}{3}\right) & \cos\left(\theta_r + \frac{2\pi}{3}\right) \\ \sin\theta_r & \sin\left(\theta_r - \frac{2\pi}{3}\right) & \sin\left(\theta_r + \frac{2\pi}{3}\right) \\ \frac{1}{2} & \frac{1}{2} & \frac{1}{2} \end{bmatrix} \tag{4.15}$$

The second is called two to three transformation, which is given by:

$$T_{abc}{}^{-1} = \begin{bmatrix} \cos\theta_r & \sin\theta_r & 1 \\ \cos\left(\theta_r - \frac{2\pi}{3}\right) & \sin\left(\theta_r - \frac{2\pi}{3}\right) & 1 \\ \cos\left(\theta_r + \frac{2\pi}{3}\right) & \sin\left(\theta_r + \frac{2\pi}{3}\right) & 1 \end{bmatrix} \tag{4.16}$$

The application of these transformations is accomplished in the following manner. Given phase voltages in stationary reference frame, the output voltages in rotor reference frame are determined by:

$$\begin{Bmatrix} v_{ds}^r \\ v_{qs}^r \\ v_\circ \end{Bmatrix} = \{T_{abc}\} \begin{Bmatrix} v_a^s \\ v_b^s \\ v_c^s \end{Bmatrix} \tag{4.17}$$

Given phase currents in rotor reference frame, the output currents in stationary reference frame are determined by:

$$\begin{Bmatrix} i_a^s \\ i_b^s \\ i_c^s \end{Bmatrix} = \{T_{abc}\}^{-1} \begin{Bmatrix} i_{ds}^r \\ i_{qs}^r \\ i_\circ \end{Bmatrix} \tag{4.18}$$

In both transformations θ_r is the rotor flux position in [rad], which is obtained by:

$$\theta_r = \int \omega_r \, dt \tag{4.19}$$

4.4 PMSM Model

The different components of PMSM SIULINK model are described in detail in this section. This model is part of a complete variable speed motor drive system. The dynamic response of the model will be introduced after the field oriented control and the maximum efficiency control strategy are completed in the next chapters.

Figure 4.5 shows the main window of PMSM model in rotor frame reference. The model inputs are v_{ds}^r, v_{qs}^r and the load torque. If the speed and current controllers are designed accurately, the electromagnetic torque has to be equal the load torque in steady state. The outputs of the model are speed, torque, position, i_{ds}^r and i_{qs}^r. The model is organized in four subsystems system 1, system 2, system 3 and system 4. Figure 4.6 illustrates system 1 in which the equations (4.2) and (4.3) are realized. Equations (4.5), (4.6) and the mechanical system equations are realized in system 2 as illustrated in Figure 4.7. It is worth mentioning that the position angle generated by the numerical integration of the mechanical system serves as input parameter for (4.5) and (4.6). The core loss currents, model input currents and mechanical system are illustrated in Figures 4.8, 4.9, and 4.10, respectively.

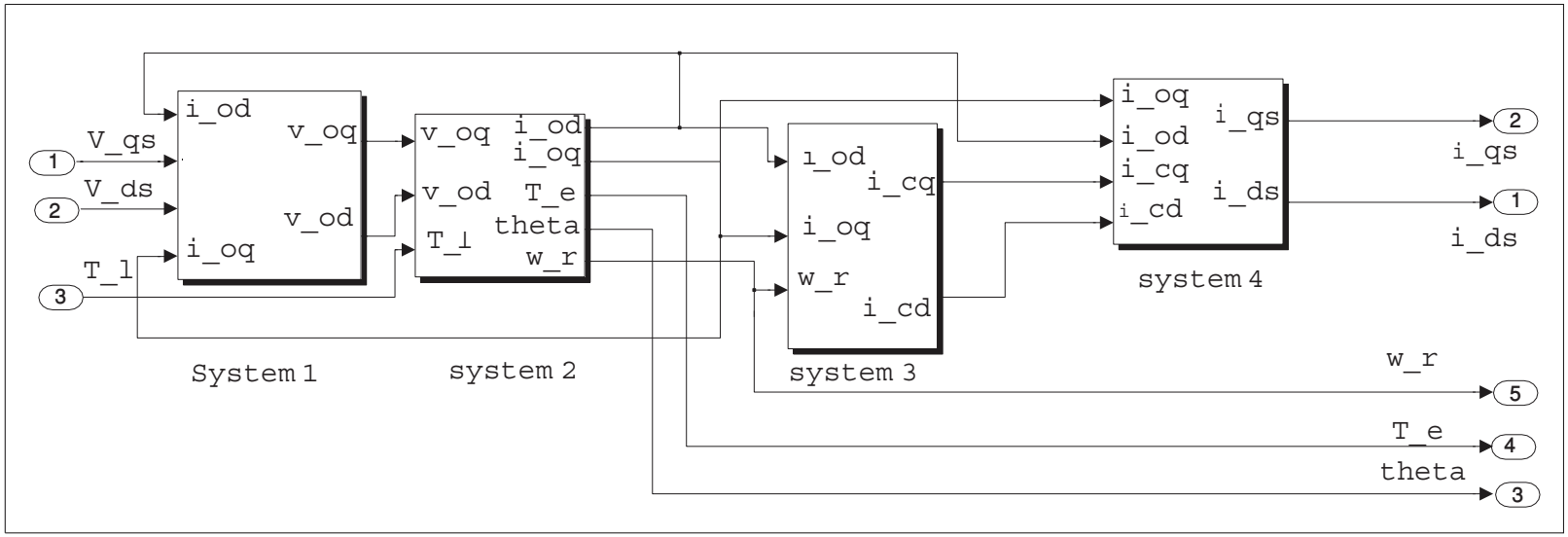

Figure 4.5: Main SIMULINK window of PMSM model in rotor reference frame.

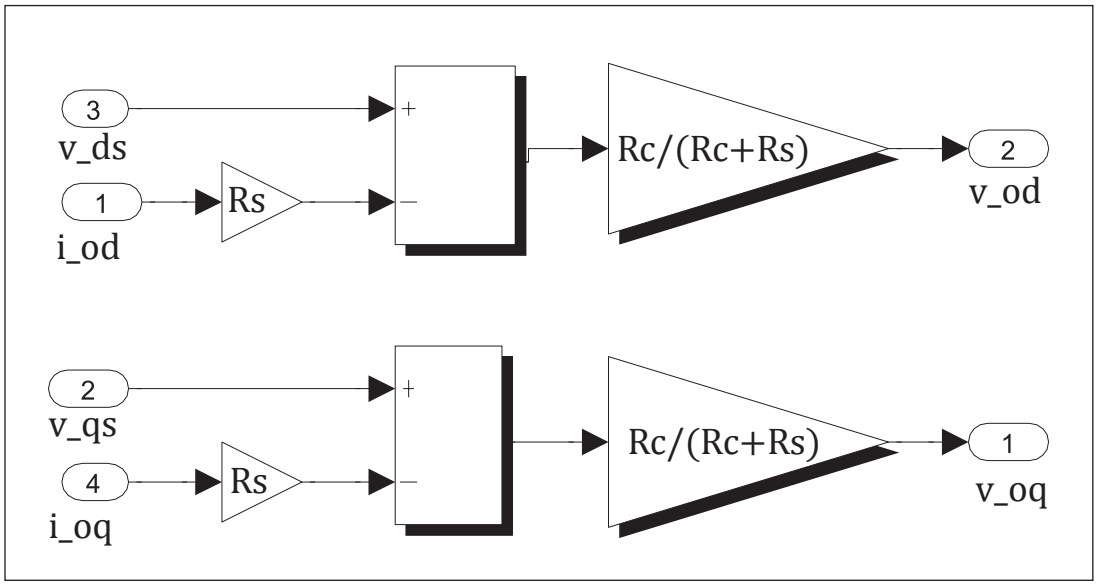

Figure 4.6: System 1 in the Main SIMULINK window of PMSM model.

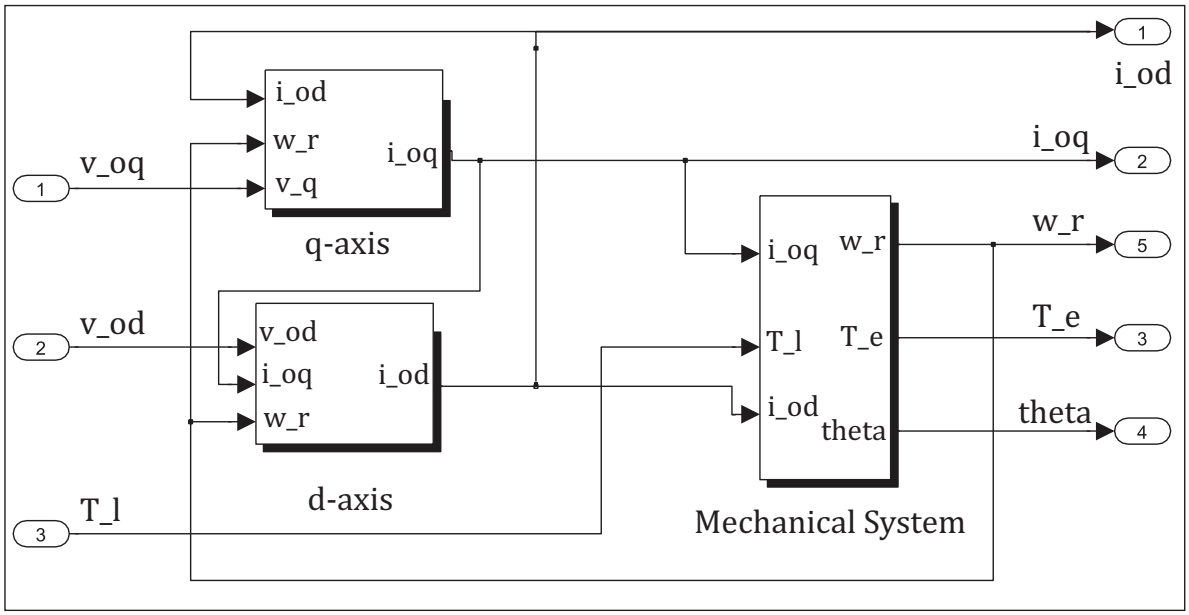

Figure 4.7: System 2 in the Main SIMULINK window of PMSM model.

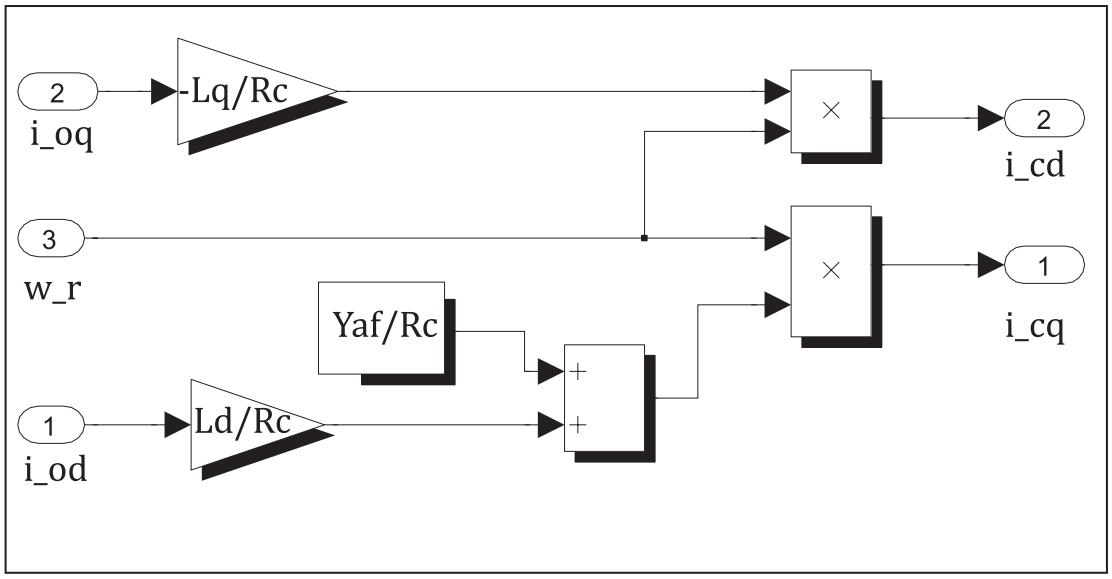

Figure 4.8: System 3 in the Main SIMULINK window of PMSM model.

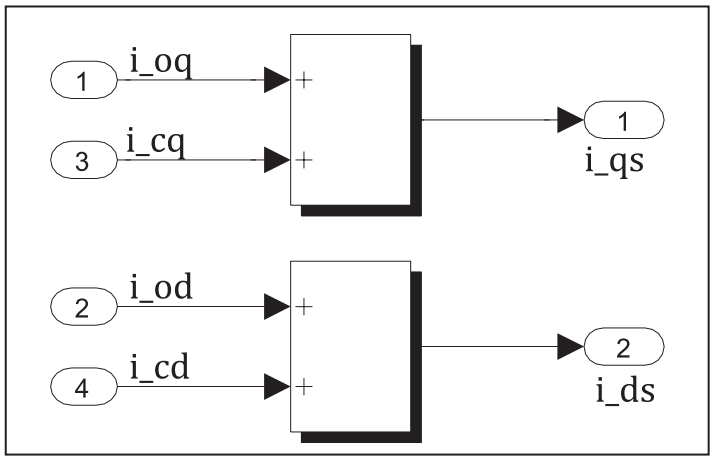

Figure 4.9: System 4 in the Main SIMULINK window of PMSM model.

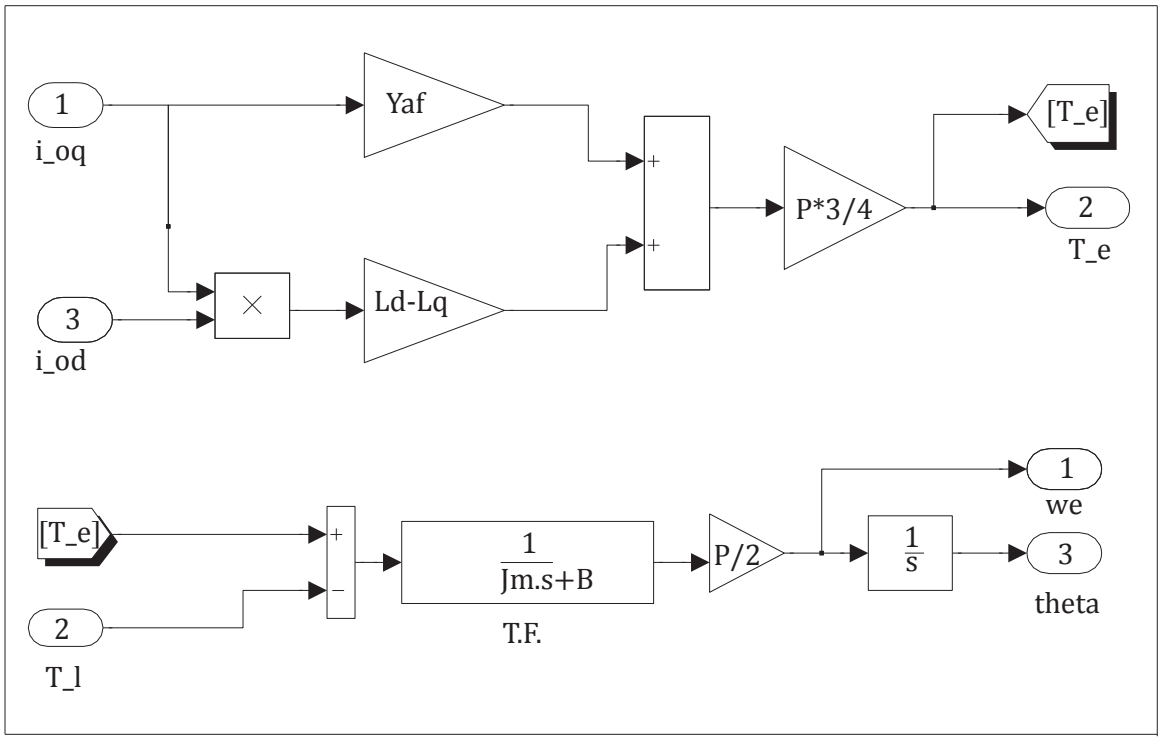

Figure 4.10: Mechanical system in the Main SIMULINK window of PMSM model.

Chapter 5

Field Orientated Control of PMSM

5.1 Introduction

Vector control, also known as decoupling or field oriented control, came into the field of ac drives research in the late 1960s. It was developed prominently in the 1980s to meet the challenges of oscillating flux and torque responses in inverter fed induction and synchronous motor drives [28]. Traditionally variable speed electric machines were based on the separately excited dc machines. The main reason was due to the high performance dynamic ability of separately excited dc machines drives that resulted from its ability of independent control of the flux and torque. The flux is controlled by the field current alone. The field current is kept constant and hence is the flux. The torque is independently controlled by the armature current alone. Therefore, this armature current may be treated as the torque-producing current. In the dc machine, this decoupling is obtained in by orienting the current in quadrature to the stator flux by use of a mechanic commutator.

In the last three decades, significant advances in the areas of power semiconductor and

control technology have led to adjustable speed-drives for ac machines. The mathematical models for ac machines are inherently more complex than the dc counterparts. More complex control schemes and more expensive power converters are needed to achieve acceptable speed and torque control performance. By use of advanced control approaches like field-oriented control, the dynamic performance at least equivalent to that of a commutator motor can be achieved. The key to it then lies in finding an equivalent flux-producing current and torque-producing current in ac machines leading to the control of the flux and torque channels in them.

To achieve the necessary decoupling, first the machine has to be modeled in space vector form, where a three-phase machine is transformed into a machine with one winding each on stator and rotor. The transformed machine resembles an equivalent dc machine. Second, the ability of the inverter to produce a current vector with controllable magnitude, frequency, and phase is needed. Both of these features are exploited to make the PMSM drive system a high-performance drive system with independent control of its mutual flux and electromagnetic torque [28]. The details are explained in the following sections.

5.2 Field Orientated Control of PMSM

A field-oriented dq control technique is one in which the d- and q-axis components of the current are controlled independently. Typically one of them is oriented to control the flux while the other is oriented to control the torque. The next subsections describe in detail the components that form field oriented controller.

5.2.1 Space Vector Definition and Projection

The three-phase voltages, currents and fluxes of ac machines can be analyzed in terms of complex space vectors [38]. The space vector of the motor input currents in stator reference frame can be defined as follows. Given the instantaneous currents i_a^s, i_b^s, i_c^s, then the complex stator current vector $\overline{i}_s^s$ is defined as:

$$\overline{i}_s^s = i_a^s + \alpha\, i_b^s + \alpha^2\, i_c^s \tag{5.1}$$

where $\alpha = e^{j\frac{2}{3}\pi}$. The diagram in Figure 5.1 illustrates the stator current complex space vector.

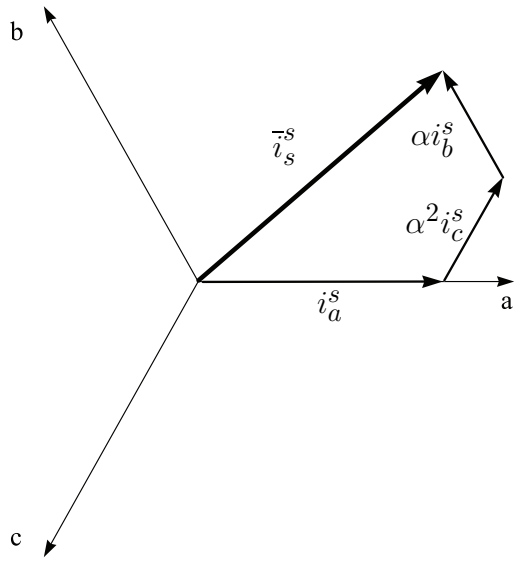

Figure 5.1: Stator current space vector and its components.

The depicted space vector current represents three-phase sinusoidal system. It still needs to be transformed into a rotating coordinate system. This transformation can be accomplished in two steps:

• $(a, b, c) \Rightarrow (\alpha, \beta)$ Clarke transformation that outputs a two coordinate time variant system.

• $(\alpha, \beta) \Rightarrow (d, q)$ Park transformation that outputs a two coordinate time invariant system.

The complete description of these transformation will be detailed in the next subsections.

5.2.1.1 Clarke Transformation

The Clarke transform takes three-phase currents i_a^s, i_b^s and i_c^s to calculate currents in the two-phase orthogonal stator axes $i_{s\alpha}$ and $i_{s\beta}$. These two currents in the stator reference frame and, mathematically represented as:

$$\begin{Bmatrix} i_{s\alpha} \\ i_{s\beta} \\ i_\circ \end{Bmatrix} = \begin{Bmatrix} \frac{2}{3} & -\frac{1}{3} & \frac{1}{3} \\ 0 & \frac{2}{\sqrt{3}} & -\frac{2}{\sqrt{3}} \\ \frac{2}{3} & \frac{2}{3} & \frac{2}{3} \end{Bmatrix} \begin{Bmatrix} i_a^s \\ i_b^s \\ i_c^s \end{Bmatrix} \tag{5.2}$$

In addition to the orthogonal components of the current space vector, the Clarke transformation matrix calculates $i_\circ$, which represents the zero-sequence component in the a, b, and c phase currents. For three-phase balanced system, there are only two independent variables in abc and the third is the dependent variable obtained as the negative sum of the other two variables [28]. Figure 5.2 shows the transformed space vector with $i_{s\alpha}$ aligned with i_a^s. If $i_a^s + i_b^s + i_c^s = 0$, i_a^s, i_b^s and i_c^s can be transformed to $i_{s\alpha}$ and $i_{s\beta}$ with the following simplified transformation:

$$\begin{Bmatrix} i_{s\alpha} \\ i_{s\beta} \end{Bmatrix} = \begin{Bmatrix} 1 & 0 \\ \frac{1}{\sqrt{3}} & \frac{2}{\sqrt{3}} \end{Bmatrix} \begin{Bmatrix} i_a^s \\ i_b^s \end{Bmatrix} \tag{5.3}$$

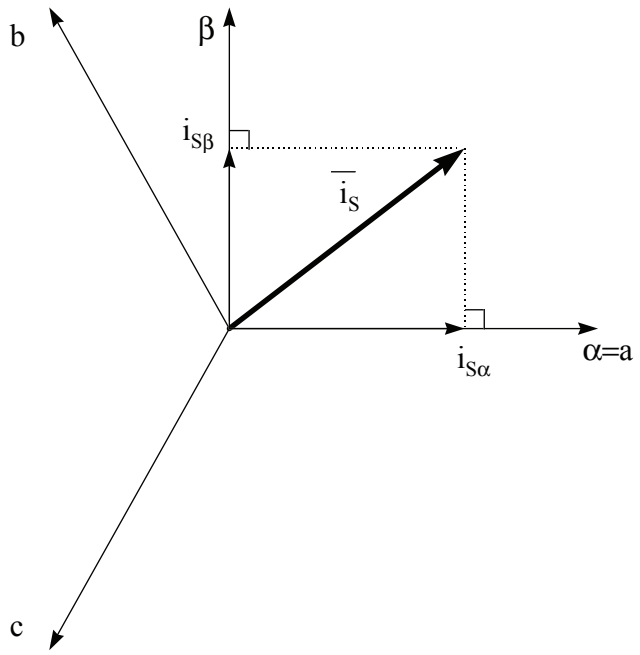

Figure 5.2: Stator current space vector and its orthogonal components.

5.2.1.2 Park Transformation

The orthogonal components of the stator currents space vector in stationary reference frame are transform to q- and d-axes stator currents in rotor reference frame through the Park transformation:

$$\begin{Bmatrix} i_{qs}^{r} \\ i_{ds}^{r} \end{Bmatrix} = \begin{Bmatrix} -\sin\theta & \cos\theta \\ \cos\theta & \sin\theta \end{Bmatrix} \begin{Bmatrix} i_{s\alpha} \\ i_{s\beta} \end{Bmatrix} \tag{5.4}$$

Herein, the d-axis is aligned with the rotor flux. Figure 5.3 shows the current vector in the stationary and rotating frames of references.

5.2.1.3 Inverse Park Transformation

This transformation accepts the space vector components of the stator voltage in rotor reference frame, and transforms them to the α β components in the stator reference frame. Equation (5.5) shows the mathematical representation of the inverse Park transformation.

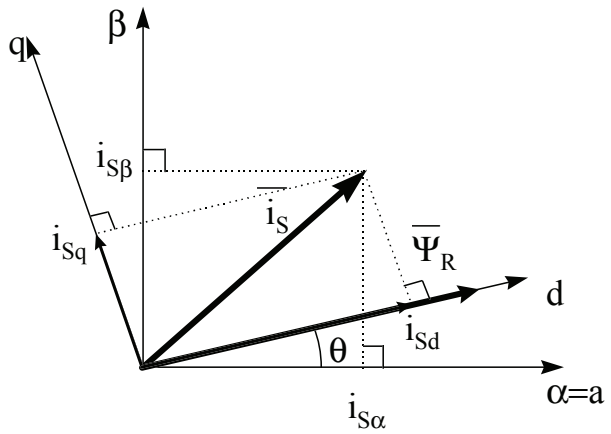

Figure 5.3: Stator current space vector and its component in the stationary and rotating reference frames.

Generation of the stator space vector represents the last step in the field oriented control scheme if the space vector modulation technique is employed. Since the sinusoidal PWM technique is used in this study, the stator space vector has to be resolved to its abc components v_a^s, v_b^s and v_c^s. Equation (5.6) represents the transformation of the space vector to its abc components in the same reference frame. The phase voltages generated by this transformation represent the commands needed to generate the gating signals, which control the switches of the VSI. It is worth mentioning that resolving the stator space vector to its components does not need the rotor position information since this transformation takes place in the same reference frame.

$$\begin{Bmatrix} v_{s\alpha}^* \\ v_{s\beta}^* \end{Bmatrix} = \begin{Bmatrix} -\sin\theta & \cos\theta \\ \cos\theta & \sin\theta \end{Bmatrix} \begin{Bmatrix} v_{qs}^{r*} \\ v_{ds}^{r*} \end{Bmatrix} \tag{5.5}$$

$$\begin{Bmatrix} v_a^{s*} \\ v_b^{s*} \\ v_c^{s*} \end{Bmatrix} = \begin{Bmatrix} 1 & 0 \\ \frac{1}{2} & \frac{\sqrt{3}}{2} \\ -\frac{1}{2} & -\frac{\sqrt{3}}{2} \end{Bmatrix} \begin{Bmatrix} v_{s\alpha}^* \\ v_{s\beta}^* \end{Bmatrix} \tag{5.6}$$

5.2.2 Overall PMSM Drive System

The implementation of the vector-controlled PMSM drive system is described in this section based on the understanding gained in the previous sections on vector control. The overall block diagram of the speed-controlled systems is illustrated in Figure 5.4. The first step is to measure two stator phase currents. These measurements are fed to the Clarke transformation module. The outputs of this module are $i_{s\alpha}$ and $i_{s\beta}$. These two components of the space vector current are the inputs of the Park transformation that gives the current in the d,q rotating reference frame. The i^r_{qs} and i^r_{ds} components are compared to the references i^{r*}_{ds} (the flux reference) and i^{r*}_{qs} (the torque reference), respectively. The torque command i^{r*}_{qs} is the output of the speed regulator and i^{r*}_{ds} is the output of the maximum efficiency control algorithm, which will be further detailed in the next chapter. The outputs of the current regulators are v^{r*}_{qs} and v^{r*}_{ds}, which are applied to the inverse Park transformation. The outputs of this projection are $v^*_{s\alpha}$ and $v^*_{s\beta}$, which are the components of the stator voltage vector in the α, β stationary orthogonal reference frame. $v^*_{s\alpha}$ and $v^*_{s\beta}$ are also the inputs of the space vector PWM modulator. However, in SPWM, the outputs of this block are resolved into components of the voltage space vector, which are subsequently compared with carrier signals to generate the signals that drive the inverter. It is worth noting that both Park and inverse Park transformations need the rotor flux position, which means increased complexity and the cost of ac drive system. The obtaining of the rotor flux position is discussed in the following subsection.

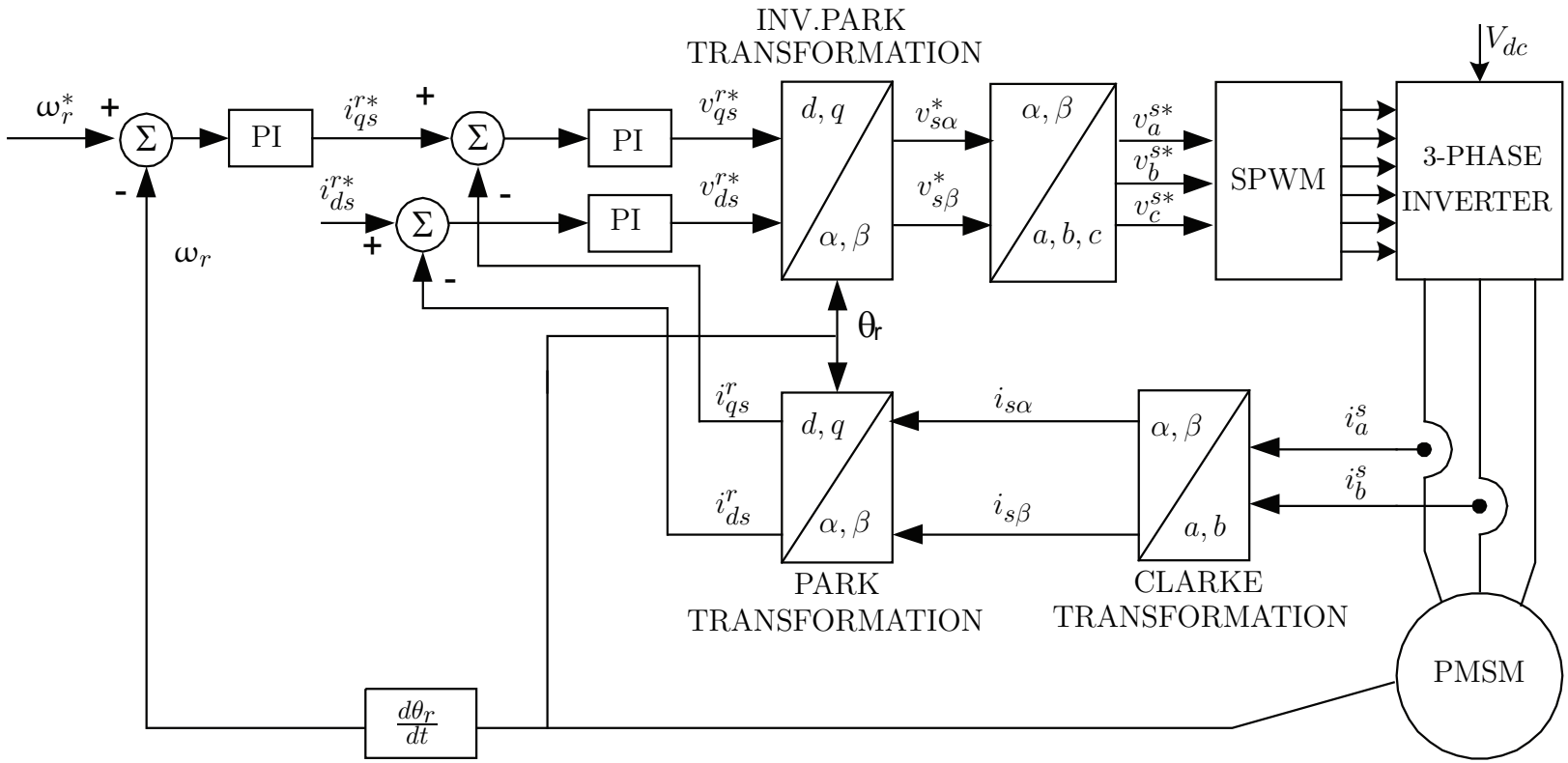

Figure 5.4: Field orientation control diagram.

5.2.3 Field Orientation Input Parameters

To implement the field oriented controller, two input variables are needed: rotor position and two of motor stator currents. As described in the last subsections, the transformation from stator to rotor reference frames and vice versa requires rotor position. The rotor position can be measured directly by position sensor or by integration of rotor speed since the rotor speed is equal to the rotor flux speed in PMSM [38]. However, the currents considered as the core variables of FOC. The currents are measured by current sensor and then sampled by A/D before received by the controller. In recent years most control algorithms are implemented in digital signal processor (DSP) because of its ability to generate the triggering signal of the voltage source inverter at very high switching frequency and its capability of implementation of even very sophisticated control algorithms.

5.3 Sinusoidal Pulse Width Modulation

In order to investigate the motor harmonics loss caused by static power conversion, the inverter topology, and control method have to be determined first. Since the power rating of the PMSM under study is about 3 kW, the three-phase inverter with IGBTs has been chosen as controlled switches as shown in Figure 5.5. However, there are different control methods that can be used to control motor speed (by the control of the frequency, amplitude and phase of motor phase voltages) such as space vector PWM (SVPWM), six-step, and sinusoidal PWM (SPWM). Despite SVPWM generate less harmonics than SPWM with higher output fundamental voltage, the spectral analysis of output voltage of SPWM inverter is a straightforward process by application of double Fourier series expansion. The next sections highlight the important aspects of controlling the three-phase VSI by SPWM control

method.

5.3.1 Sinusoidal Pulse Width Modulated Inverter Model

The VSI consist of three legs connected in parallel, and is supplied with a constant dc voltage as shown in Figure 5.5. Each leg consists of two IGBT switches connected in series and is controlled by pluses obtained by the comparison between the reference command and the triangle carrier waveform. It is important to note that the two IGBTs in the same leg is never conducting simultaneously since in such shoot-through case high short-circuit current passes through the leg leads to damage of the inverter module. If ideal transistors in the inverter module are assumed, then there is no short circuit as long as there is no overlap between the upper and lower switches. However, practical inverters will need deadtime to avoid shoot-through since finite time interval is needed for the commutation of these semiconductor power switches.

The triangle waveform named carrier determines the converter switching frequency. The frequency of the reference command establishes the desired fundamental frequency of the inverter output voltage. The frequency ratio of the carrier waveform to the reference command is referred to as the frequency modulation ratio. The ratio between the amplitude of the fundamental component and the amplitude of the carrier signal is called modulation index. The diodes in the circuit diagram provide paths for currents when a transistor is gated on but cannot conduct the polarity of the load current [39]. For example, if the load current is negative when the upper transistor is gated on, the diode in parallel with the upper transistor will conduct until the load current becomes positive at which time the upper transistor will begin to conduct. The switches of the phase legs are controlled based on the following

comparison:

$$v_a^{s*} \geq v_{tr}\ T1\ is\ on$$

$$v_a^{s*} < v_{tr}\ T2\ is\ on$$

$$v_b^{s*} \geq v_{tr}\ T3\ is\ on$$

$$v_b^{s*} < v_{tr}\ T6\ is\ on$$

$$v_c^{s*} \geq v_{tr}\ T5\ is\ on$$

$$v_c^{s*} < v_{tr}\ T4\ is\ on$$

where v_a^{s*}, v_b^{s*} and v_c^{s*} are the reference control commands generated by by control algorithm. v_{tr} is the triangle waveform. The mathematical derivation of the inverter output phase and line voltages will be detailed in the next subsection.

5.3.2 Basic Operation of SPWM Inverter

The dc link voltage is assumed constant in the three-phase voltage source inverter shown in Figure 5.5. The midpoints of the inverter phase-legs are a, b, and c. The inverter output voltages with respect to negative rail of the dc bus have two output states each:

$$\begin{aligned} v_{ag} &= V_{dc} \text{ for } T1 \text{ on and } T2 \text{ off} \\ &= 0 \quad \text{for } T2 \text{ on and } T1 \text{ off} \\ v_{bg} &= V_{dc} \text{ for } T3 \text{ on and } T6 \text{ off} \\ &= 0 \quad \text{for } T6 \text{ on and } T3 \text{ off} \\ v_{cg} &= V_{dc} \text{ for } T5 \text{ on and } T4 \text{ off} \\ &= 0 \quad \text{for } T4 \text{ on and } T5 \text{ off} \end{aligned}$$

They are derived with the assumption that the devices are ideal. The line-to-line voltages can be derived as:

$$v_{ab} = v_{ag} - v_{bg}$$

$$v_{bc} = v_{bg} - v_{cg}$$

$$v_{ca} = v_{cg} - v_{ag}$$

For balanced system in which the sum of currents and voltages equals zero, the phase voltages can be expressed as the following:

$$v_{an} = \frac{1}{3}\left(v_{ab} - v_{ca}\right)$$

$$v_{bn} = \frac{1}{3}\left(v_{bc} - v_{ab}\right)$$

$$v_{cn} = \frac{1}{3}\left(v_{ca} - v_{bc}\right)$$

Let the modulation index be defined as:

$$M = \frac{\hat{V}_{ref}}{\hat{V}_{tri}} \tag{5.7}$$

If $M \leq 1$, the modulation is linear, where the fundamental frequency component in the output voltage varies linearly with the amplitude modulation index ratio M [40]. From Figure 5.6, the peak value of the fundamental-frequency component in one of the inverter legs is:

$$\left(\hat{V}_{ag}\right)_1 = M\frac{V_{dc}}{2} \tag{5.8}$$

Therefore the line-to-line rms voltage at the fundamental frequency, due to 120° phase displacement between phase voltages, can be written as:

$$\begin{aligned} V_{LL} &= \frac{\sqrt{3}}{\sqrt{2}}\left(\hat{V}_{ag}\right)_1 \\ &= \frac{\sqrt{3}}{2\sqrt{2}} M\, V_{dc} \\ &\simeq 0.612\, M\, V_{dc} \end{aligned} \tag{5.9}$$

When $M = 1$ the maximum output line-to-line rms equals 0.612 of the dc link voltage.

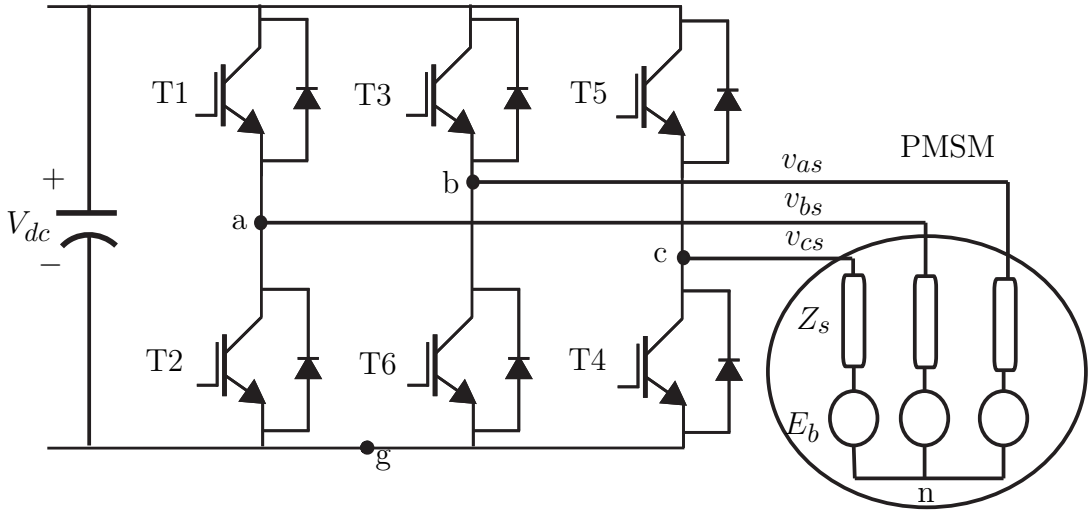

Figure 5.5: Three phase voltage source inverter circuit diagram.

Figure (5.6) shows the normalized line to line and phase to neutral VSI output voltages. The complete SIMULINK model of the VSI is shown in Figure (5.7).

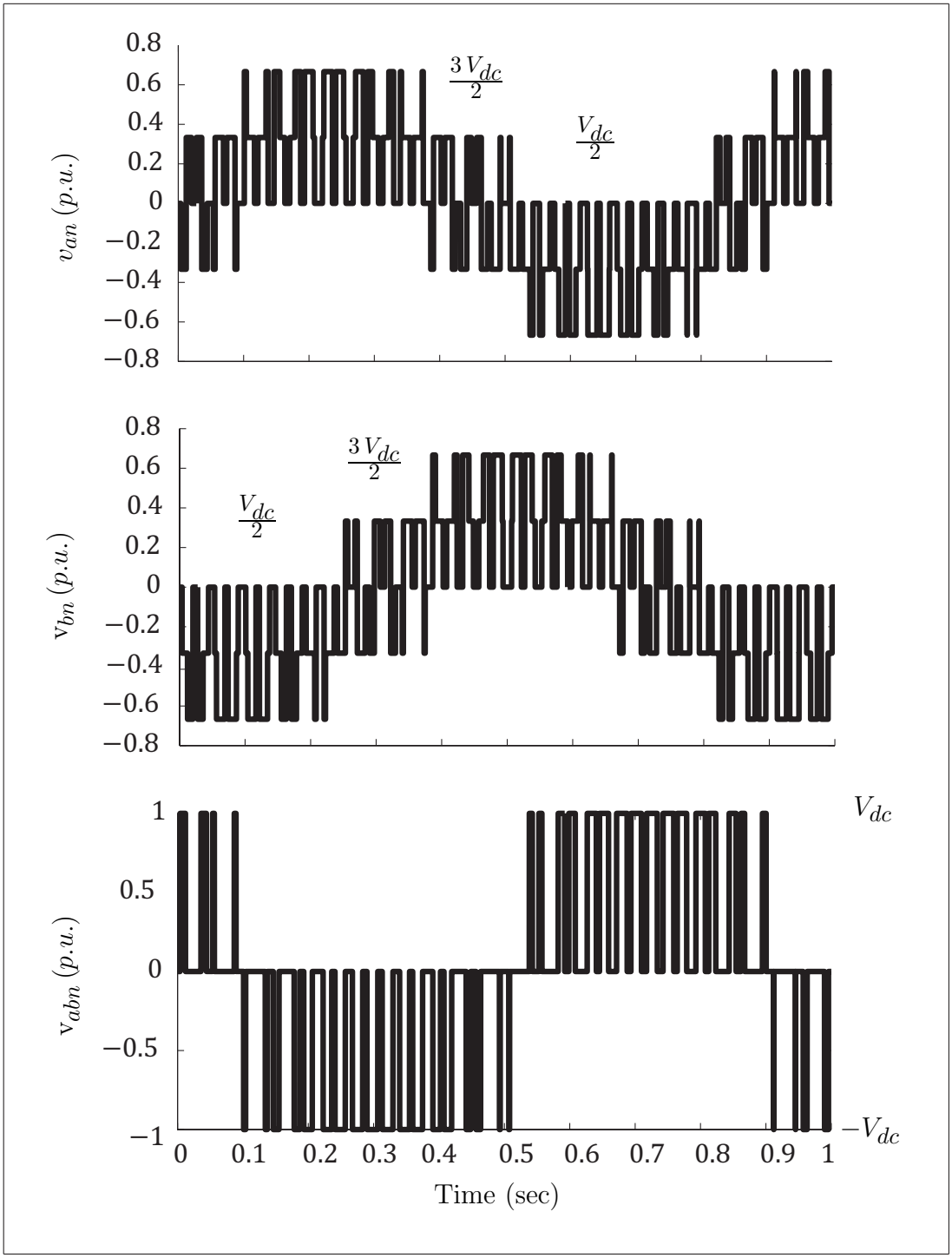

Figure 5.6: Voltage waveforms of three-phase voltage source inverter in normalized units.

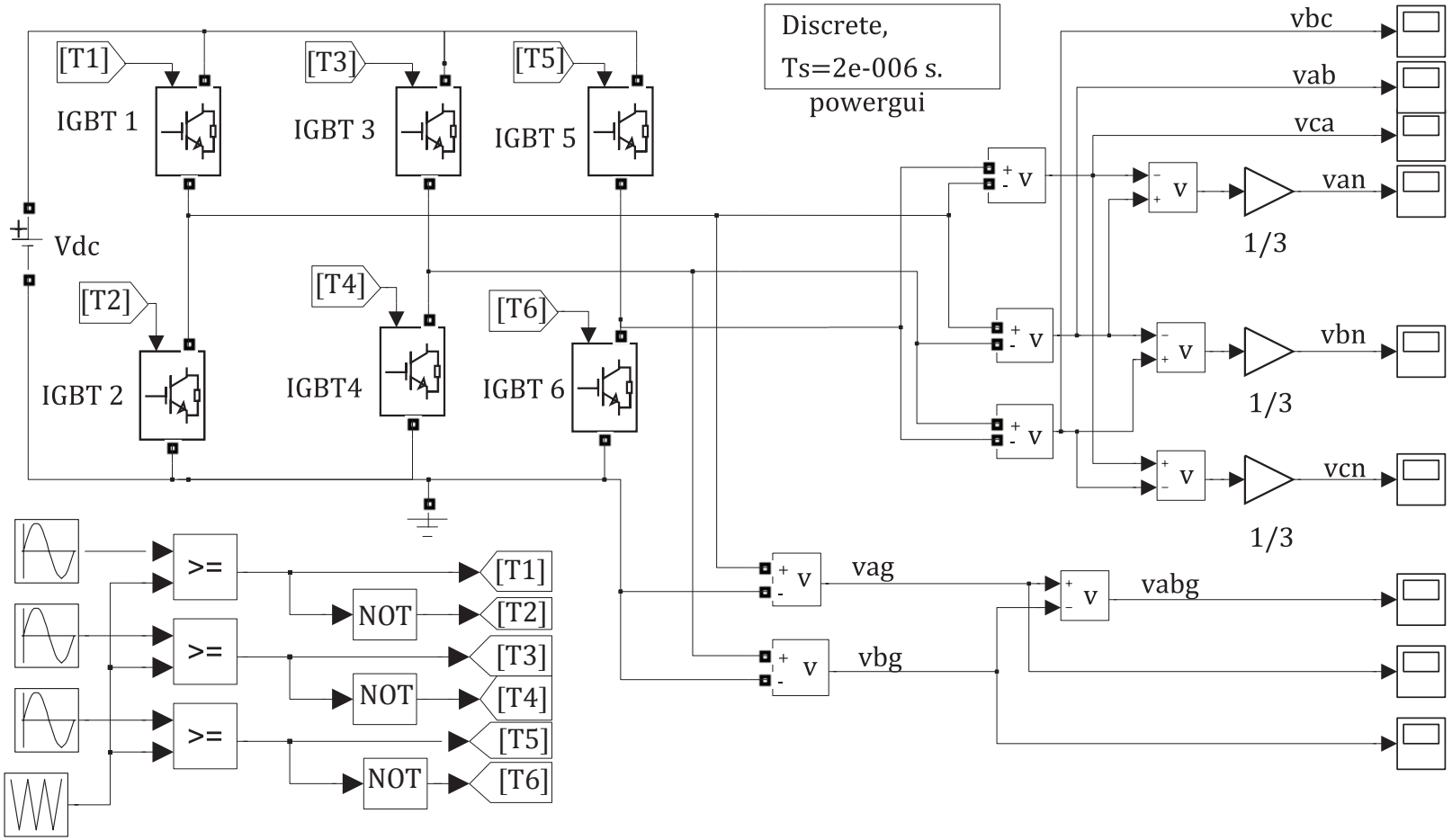

Figure 5.7: Three phase voltage source inverter implementation in SIMULINK software.

Chapter 6

Loss Minimization Control Strategy

This chapter is focused on the improvement of the efficiency of surface mounted PMSM. The combined copper losses and iron fundamental losses are minimized through control strategy developed in [41]. The controllable losses can be minimized by proper choice of the armature current vector. It is a common practice to set the current $i_d = 0$. As a result, the armature current vector that is in phase with the back EMF is applied. In addition, irreversible demagnetization of permanent magnets can be avoided [41]. The recent development of the permanent magnets has brought materials with high coercivity and high residual magnetism. Therefore, several control methods have been proposed to improve the performance of the PM motor drives. In such control methods, the d-axis component of armature current is actively controlled according to the operating speed and load conditions. In the next section, the basic equations of motor model needed to develop the control algorithm are presented.

6.1 Modeling Fundamental Losses of PMSM

Figure 6.1 shows the steady state d, q model of PMSM. The fundamental iron loss consists of hysteresis loss and eddy current loss. Herein, these two loss components are lumped into a single quantity, which is represented by the core loss resistance R_c. As shown in Figure 6.1, the voltage equations of PMSM in steady-state are expressed as:

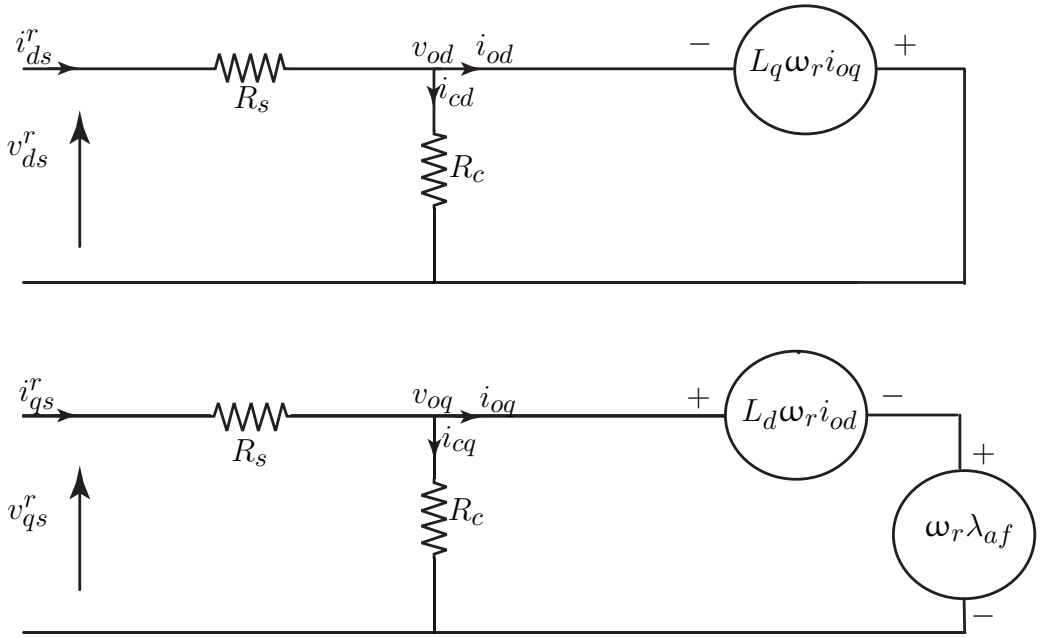

Figure 6.1: Steady state equivalent circuits of PMSM include core loss resistance.

$$\begin{bmatrix} v^r_{ds} \\ v^r_{qs} \end{bmatrix} = R_s \begin{bmatrix} i_{od} \\ i_{oq} \end{bmatrix} + \left(\frac{R_c + R_s}{R_c} \right) \begin{bmatrix} v_{od} \\ v_{oq} \end{bmatrix} \tag{6.1}$$

$$\begin{bmatrix} v_{od} \\ v_{oq} \end{bmatrix} = \begin{bmatrix} 0 & -L_q\,\omega_r \\ L_d\,\omega_r & 0 \end{bmatrix} \begin{bmatrix} i_{od} \\ i_{oq} \end{bmatrix} + \begin{bmatrix} 0 \\ \omega_r\,\lambda_{af} \end{bmatrix} \tag{6.2}$$

where

$$i_{od} = i^r_{ds} - i_{cd} \tag{6.3}$$

$$i_{oq} = i^r_{qs} - i_{cq} \tag{6.4}$$

$$i_{cd} = -\left(\frac{L_q}{R_c}\right)\omega_r\, i_{oq} \tag{6.5}$$

$$i_{cq} = \frac{1}{R_c}\left(\lambda_{af} + L_d\, i_{od}\right)\omega_r \tag{6.6}$$

The armature current i_a, the terminal voltage v_a and the torque T_e are expressed as:

$$i_a = \sqrt{i_d^2 + i_q^2} \tag{6.7}$$

$$v_a = \sqrt{v_d^2 + v_q^2}$$

$$v_a = \sqrt{\left(R_s\, i_d - \omega_r\, L_q\, i_{oq}\right)^2 + \left(R_s\, i_q + \omega_r\left(\lambda_{af} + L_d\, i_{od}\right)\right)^2} \tag{6.8}$$

$$T_e = \frac{3}{2}\frac{P}{2}\left[\lambda_{af}\, i_{oq} + \left(L_d - L_q\right) i_{od}\, i_{oq}\right] \tag{6.9}$$

The copper loss P_{Cu}, the iron loss P_{Fe} and the mechanical loss P_M, are determined by:

$$\begin{aligned} P_{Cu} &= \tfrac{3}{2} R_s\, i_a^2 \\ &= \tfrac{3}{2} R_s\, \left(i_d^2 + i_q^2\right) \\ &= \frac{3}{2} R_s \left\{ \left(i_{od} - \frac{\omega_r L_q i_{oq}}{R_c}\right)^2 + \left(i_{oq} + \frac{\omega_r\left(\lambda_{af} + L_d i_{od}\right)}{R_c}\right)^2 \right\} \end{aligned} \tag{6.10}$$

$$\begin{aligned} P_{Fe} &= \tfrac{3}{2} R_c\, i_c^2 \\ &= \tfrac{3}{2} R_c \left(i_{cd}^2 + i_{cq}^2\right) \\ &= \frac{3}{2}\left\{ \frac{\omega_r^2\left(L_q i_{oq}\right)^2}{R_c} + \frac{\omega_r^2\left(\lambda_{af} + L_d i_{od}\right)^2}{R_c} \right\} \end{aligned} \tag{6.11}$$

$$
\begin{aligned}
P_M &= T_m \omega_m \\
&= (B\omega_m)\,\omega_m \\
&= B\omega_m^2 \\
&= B\left(\frac{2}{P}\omega_r\right)^2
\end{aligned} \tag{6.12}
$$

The electrical loss P_E, the total loss P_L, the output power $P_\circ$ and the efficiency η are expressed as:

$$P_E = P_{Cu} + P_{Fe} \tag{6.13}$$

$$P_L = P_E + P_M \tag{6.14}$$

$$P_\circ = T_e\,\omega_m \tag{6.15}$$

$$\eta = \frac{P_\circ}{P_\circ + P_L} \times 100 \tag{6.16}$$

6.2 Condition for Minimized Losses

Substituting (6.10) and (6.11) into (6.13) yields an expression for controllable electrical loss as a function of ω_r, i_{od} and i_{oq}. The variable i_{oq} in these equations can be cancelled by substituting (6.9) into (6.10) and (6.11). As a result P_E can be expressed as a function of i_{od}, T_e and ω_r. In the steady state the electrical loss P_E is function of i_{od}. Nevertheless, for surface mounted PMSM $L_d = L_q$. Hence, simple expression for P_E can yield. By differentiation of P_E with respect to i_{od}, the condition for i_{od} that minimizes the controllable

losses results as:

$$\frac{\partial P_E}{\partial i_{od}} = \lambda_{af}^3 \left(\frac{3}{2}\frac{P}{2}\right)^2 i_{od} \left(R_s R_c^2 + \omega_r^2 L_d^2 R_s + \omega_r^2 L_d^2 R_c\right) + \lambda_{af}^4 \left(\frac{3}{2}\frac{P}{2}\right)^2 L_d (R_s + R_c)\omega_r^2$$
$$\frac{\partial P_E}{\partial i_{od}} = 0$$

$$i_{od} = -\frac{\lambda_{af}(R_s + R_c)\omega_r^2 L_d}{R_s R_c^2 + \omega_r^2 L_d^2 (R_s + R_c)} \tag{6.17}$$

The complete implementation of the loss minimization algorithm in SIMULINK software

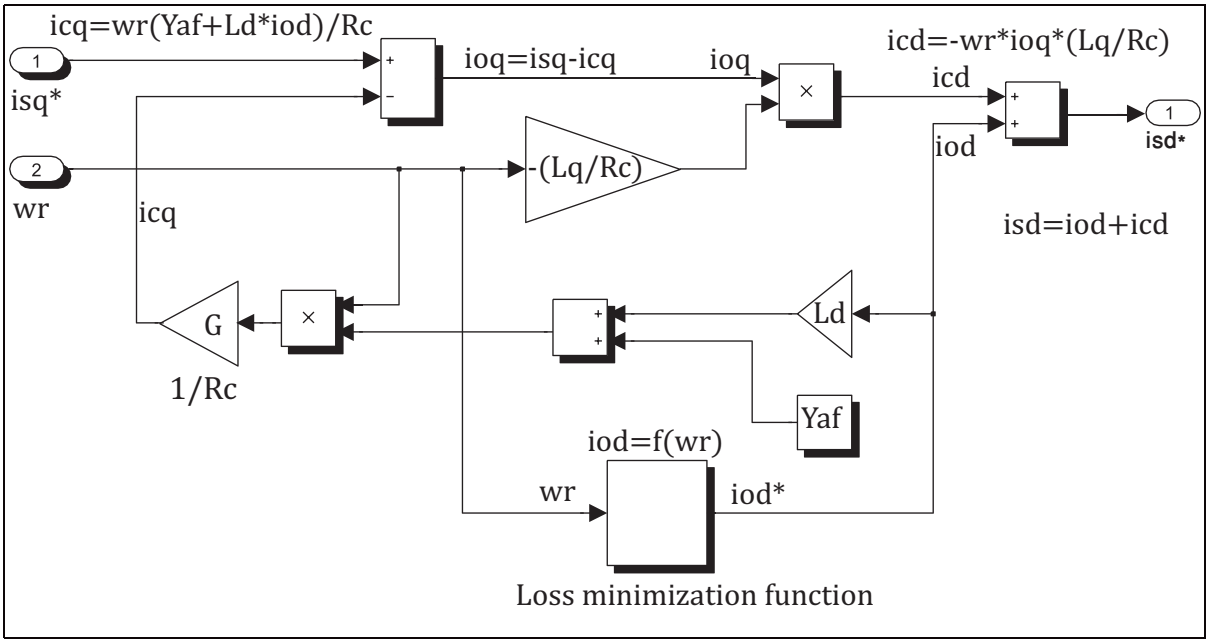

Figure 6.2: Loss minimization algorithm.

is shown in Figure 6.2. Its role in field oriented control system is shown in Figure 6.3. The simulation results will be presented in next chapter.

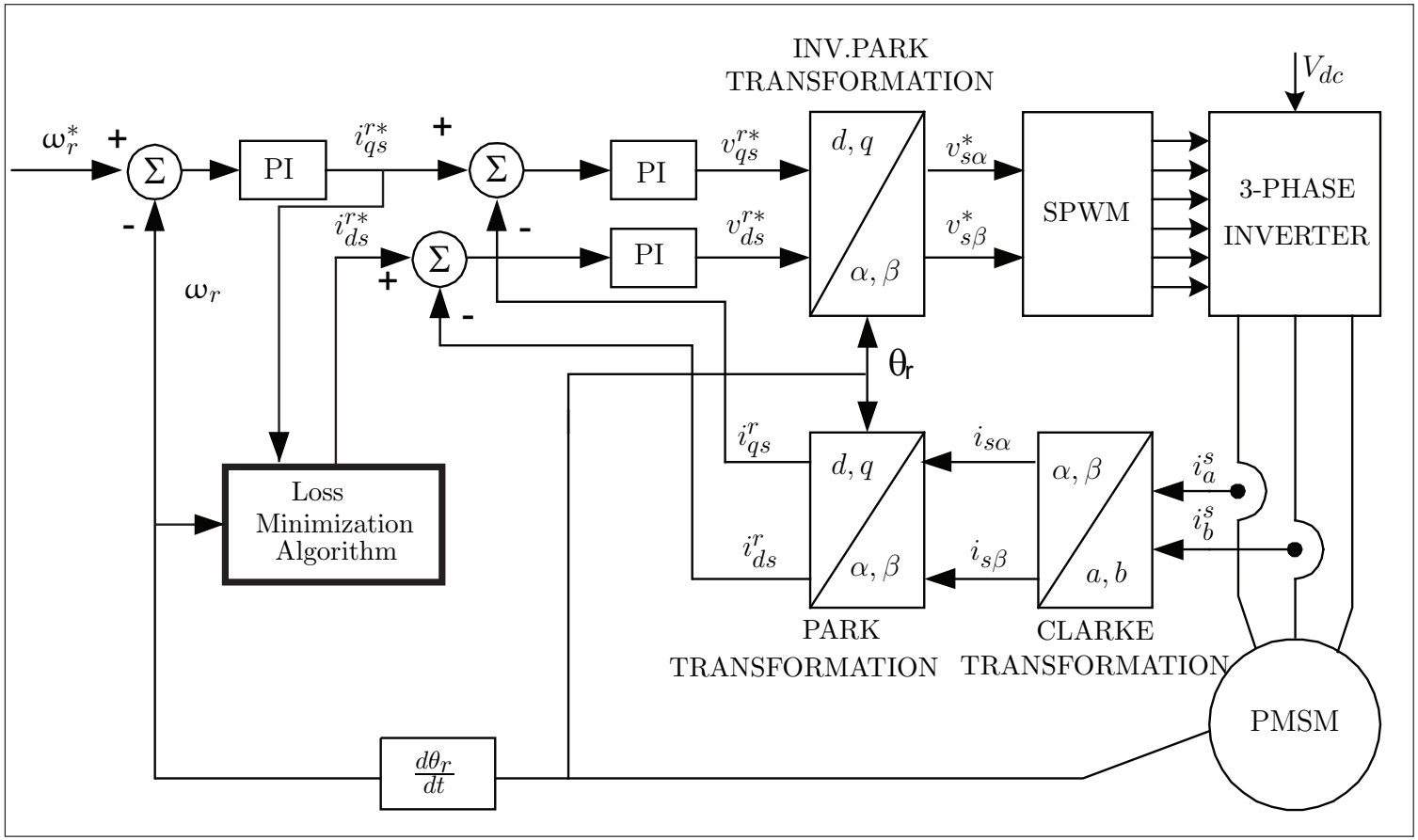

Figure 6.3: Field orientation control diagram incldues loss minimization algorithm.

Chapter 7

Simulation Results and Discussion

The machine parameters of surface mounted PMSM that have been used in the simulation are listed in Table 7.1. The field oriented control system includes the loss minimization algorithm implemented in MATLAB/SIMULINK. The Motor harmonic losses of the machine are calculated by MATLAB block using the variables that is obtained from SIMULINK for various operation conditions. The converter losses are calculated directly by use of

Table 7.1: Machine parameters.

Parameter	Value	Units
Number of pole pairs	4	
Stator resistance	0.52	ω
Core loss resistance	450	ω
Rated speed	4500	rpm
Rated torque	6	Nm
Rotor flux linkages	0.08627	Wb
Rated peak voltage per phase	150	V
Rotor inertia J_m	0.00036179	kgm^2
Viscous friction coefficient B˙m	9.444×10^{-5}	Nms
L_d	0.0013	H
L_q	0.0013	H

SIMULINK system with parameters that are generated by FOC subsystem. The results and

discussion are presented in three sections; FOC under loss minimization control strategy (LMCS), VSI-motor fundamental losses, and VSI-motor harmonic losses.

7.1 FOC with Loss Minimization Control

The dynamic responses of currents, speed and torque at rated conditions are shown in Figures 7.1 and 7.2, respectively. The system reaches the steady state with smooth dynamic response in approximate 0.14 second for the system parameters listed in Table 7.1. The current and speed controllers are designed by a symmetric optimum approach which is addressed in [28]. For calculation of the core loss resistance, it is required that the motor runs at rated speed and torque of sinusoidal power supply such that the harmonic losses are not generated. The fundamental iron loss P_{Fe} is calculated by subtracting the mechanical and copper losses from the total output power. The iron loss resistance, R_c, can be obtained from fundamental core losses as in equation (6.11), where the measured R_c represents the iron loss resistance at the rated output power. Practically R_c depends on operating conditions. However, it is assumed constant in this work.

Figure 7.3 shows the efficiency of surface mounted PMSM versus speed for the two control strategies: zero i_d control strategy and (LMC) strategy. It is clear that the motor efficiency under maximum efficiency control strategy is higher than the efficiency under zero i_d control strategy. However, the difference in efficiency is not as remarkable for surface mounted PMSM as for interior PMSM due to the following reasons. In interior PMSM The negative d-axis current produces a positive reluctance torque due to the saliency ($L_d < L_q$), and accordingly the stator current and the copper loss P_{Cu} is smaller compared with the $i_d = 0$ control. Moreover, in both types of PMSMs the negative d-axis current reduces the flux

linkage. Consequently, the voltage V, and the iron loss P_{Fe}, are smaller as compared with

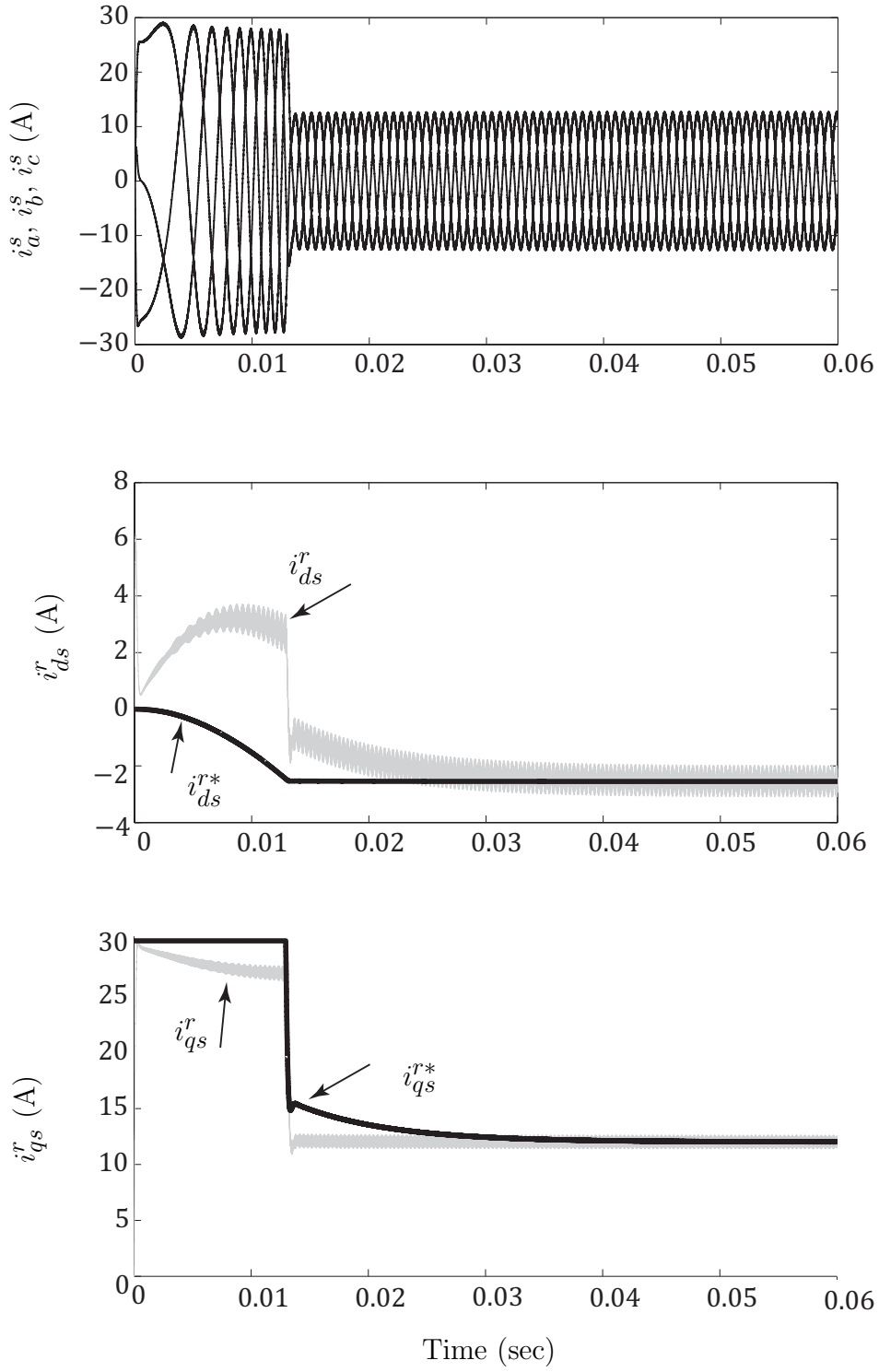

Figure 7.1: Dynamic response of phase currents, i_d and i_q of surface mounted PMSM.

the $i_d = 0$ control strategy [41]. Since the surface mounted PMSM has no saliency ($L_d = L_q$), there is no reluctance torque. However, the influence of the decreased flux linkage and applied voltage is still effective.

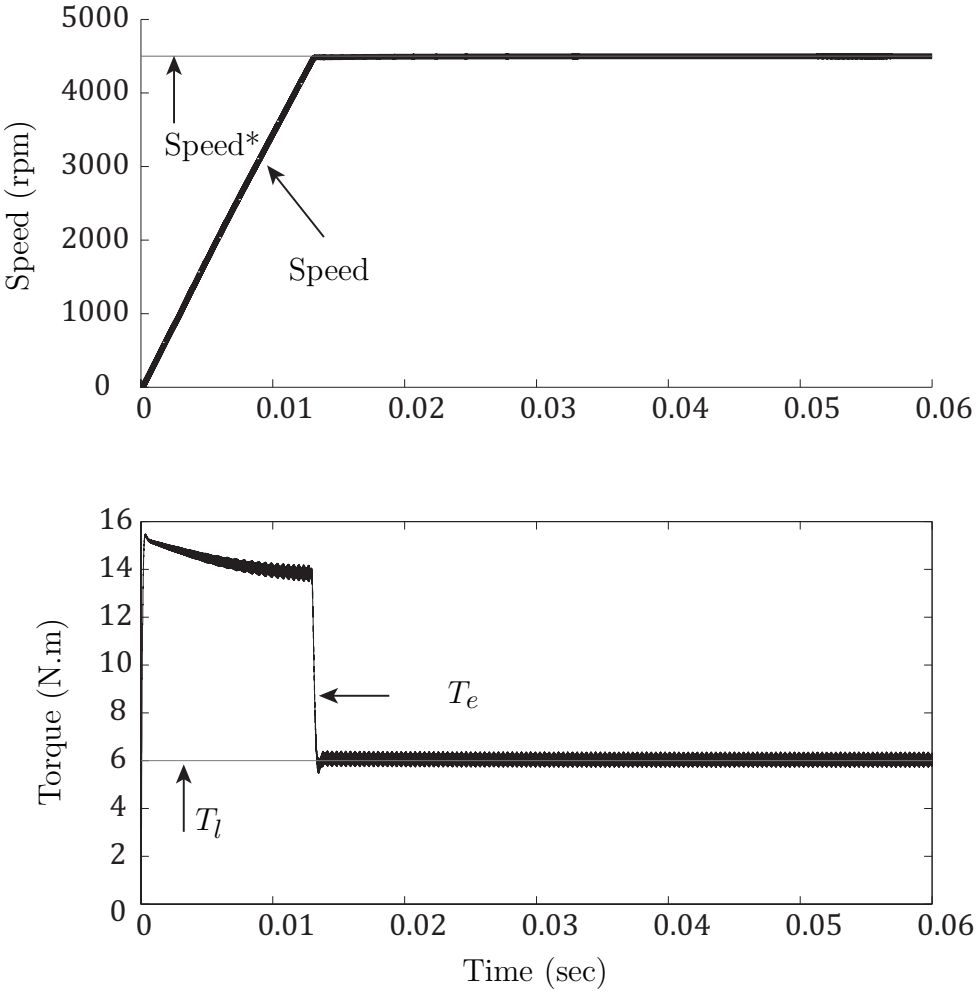

Figure 7.2: Torque and speed dynamic response of surface mounted PMSM.

7.2 VSI and PMSM Fundamental Losses

As presented in Chapter 3, the losses of VSI are divided into two types; conduction losses and switching losses. Equation (3.5) shows that the switching loss is proportional to switch-

ing frequency and motor phase current. Hence, if the motor is controlled under constant switching frequency, the switching losses are proportional to motor phase current. However, motor current increases/decreases for any increase/decrease in load torque or/and reference speed. As a result, the switching loss increases/decreases for any increases/decreases in load torque or/and reference speed. Alternatively, the conduction loss given in Equations (3.9) and (3.10) is proportional to motor phase current, modulation index and the displacement

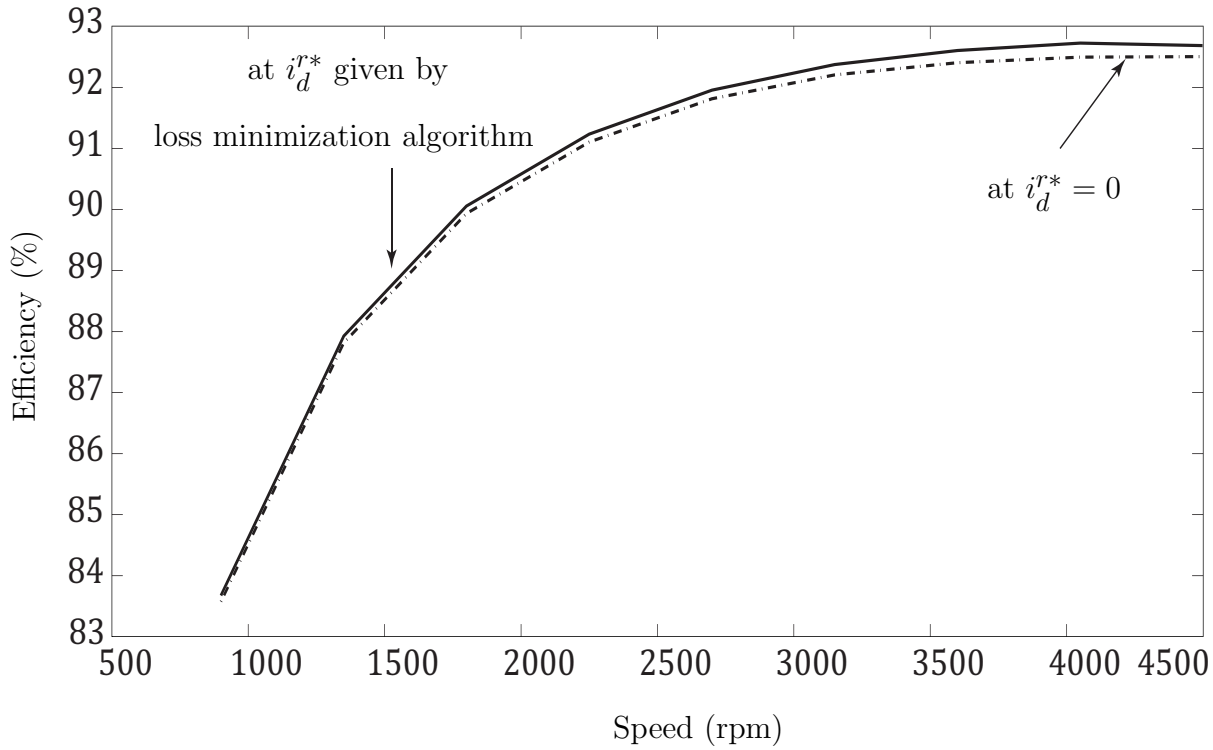

Figure 7.3: PMSM efficiency versus speed.

angle. The modulation index is controlled by load and speed since any increase in load or speed requires higher current which is supplied via higher voltage. Therefore the modulation index increases as well to supply the required voltage. Regarding the displacement angle, its effect on conduction loss is discussed in Chapter 3. Figure 7.4 (a) illustrates the relationship

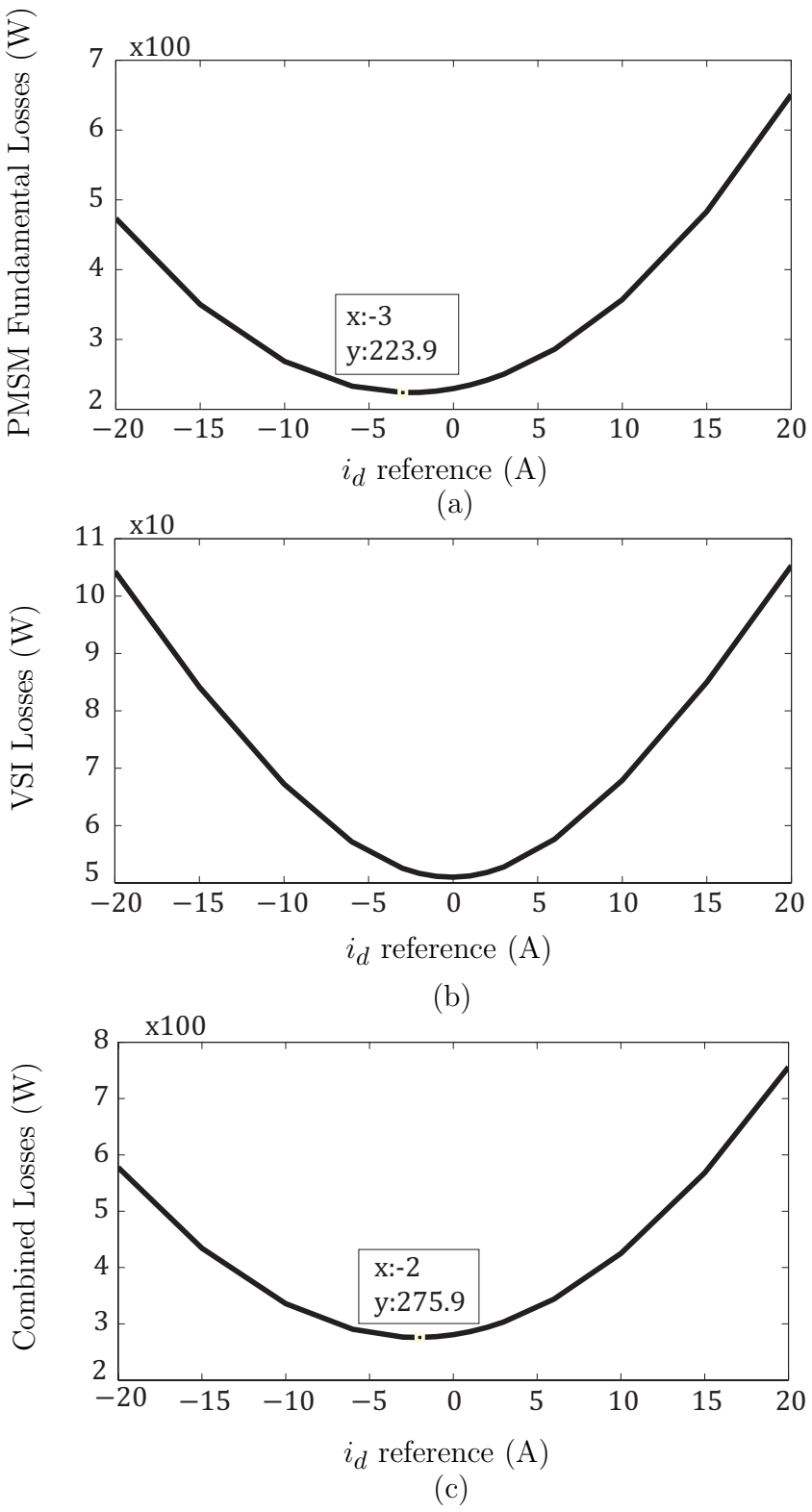

Figure 7.4: Motor-inverter fundamental losses versus i_d^{r*} at rated speed; (a) PMSM fundamental losses; (b) VSI losses; (c) Combined fundamental losses of PMSM and VSI.

between motor fundamental loss and i_d^r under loss minimization control strategy. The curve is convex with global minimum loss point at $i_d^r = -2.6\,\mathrm{A}$ for the given parameter in Table 7.1. Figure 7.4 (b) shows the relationship between the inverter losses and i_d^r. The result shows that the minimum loss point occurs at $i_d^r = 0$. This result can be explained as following: the rms value of the phase current is $\sqrt{i_d^2 + i_q^2}$. When $i_d = 0$, it is clear that the phase current has the minimum value. However, it was explained that most inverter loss is controlled by the current. When the phase current is minimum the inverter loss will be minimum as well. Figure 7.4 (c) shows the relationship between the combined losses of motor and inverter versus i_d^r. The relationship shows that the combined minimum loss value of inverter and motor occurs at a point of i_d^r that lies between the zero i_d^r and the optimal i_d^r that is generated by loss minimization algorithm.

For all conditions of loads and speeds, it can be observed that the inverter minimum loss value occurs at zero i_d^r, and the i_d^r generated by loss minimization algorithm is always negative for the same conditions. Moreover, the combined minimum loss value will strictly lie in the region between zero i_d^r and i_d^r generated by minimum loss algorithm.

7.3 VSI and PMSM harmonic losses

The motor harmonic losses at any operating point can be calculated as the following. First The machine operates at rated speed and torque off sinusoidal power supply. The input power is then measured and the copper losses and output power are calculated, which gives motor efficiency and fundamental core losses. The same procedure is repeated except that the motor is supplied with SPWM-variable speed drive controller under the same torque and speed conditions. The core losses that are calculated with SPWM represent the summation

of fundamental and harmonic losses at rated output power. Subtracting the sinusoidal-core losses from SPWM-core losses yields the motor harmonics loss at rated torque and speed. At $T_e = 6$ N $\cdot$ m and N = 4500 rpm the calculated harmonics loss is 90.8445 W. However, the motor efficiency is reduced from 92.68 to 90 % when switching the sinusoidal supply with SPWM-variable speed drive controller. In PMSM the hysterics losses are very small and can be neglected. In this work the hysterics losses value is assumed to be 5% of the total harmonic losses.

$$P_{e,h} = 0.95 P_{c,h} \tag{7.1}$$

$$P_{h,h} = 0.05 P_{c,h} \tag{7.2}$$

The next step is to calculate the loss coefficients K_{em} and K_{hm} :

$$K_{em} = \frac{P_{e,h}}{\sum_{m=1}^{\infty} \sum_{n=-\infty}^{\infty} \left(\omega_{m,n} \left| I_{m,n} \right|_{f \neq f_\circ} \right)^2} \tag{7.3}$$

$$K_{hm} = \frac{P_{h,h}}{\sum_{m=1}^{\infty} \sum_{n=-\infty}^{\infty} \left(\omega_{m,n} \left| I_{m,n} \right|_{f \neq f_\circ} \right)^2} \tag{7.4}$$

The calculated values are $K_{em} = 3.8729 \times 10^{-8}$ and $K_{hm} = 0.0013$. The harmonic losses equation in W for any operating condition is:

$$\begin{aligned} P_{c,h} = {} & 3.8729 \times 10^{-8} \sum_{m=1}^{\infty} \sum_{n=-\infty}^{\infty} \left(\omega_{m,n} \left| I_{m,n} \right|_{f \neq f_\circ} \right)^2 \\ & + 0.0013 \sum_{m=1}^{\infty} \sum_{n=-\infty}^{\infty} \omega_{m,n} \left(\left| I_{m,n} \right|_{f \neq f_\circ} \right)^2 \end{aligned} \tag{7.5}$$

The motor harmonics loss, VSI loss and the total loss versus switching frequency are shown

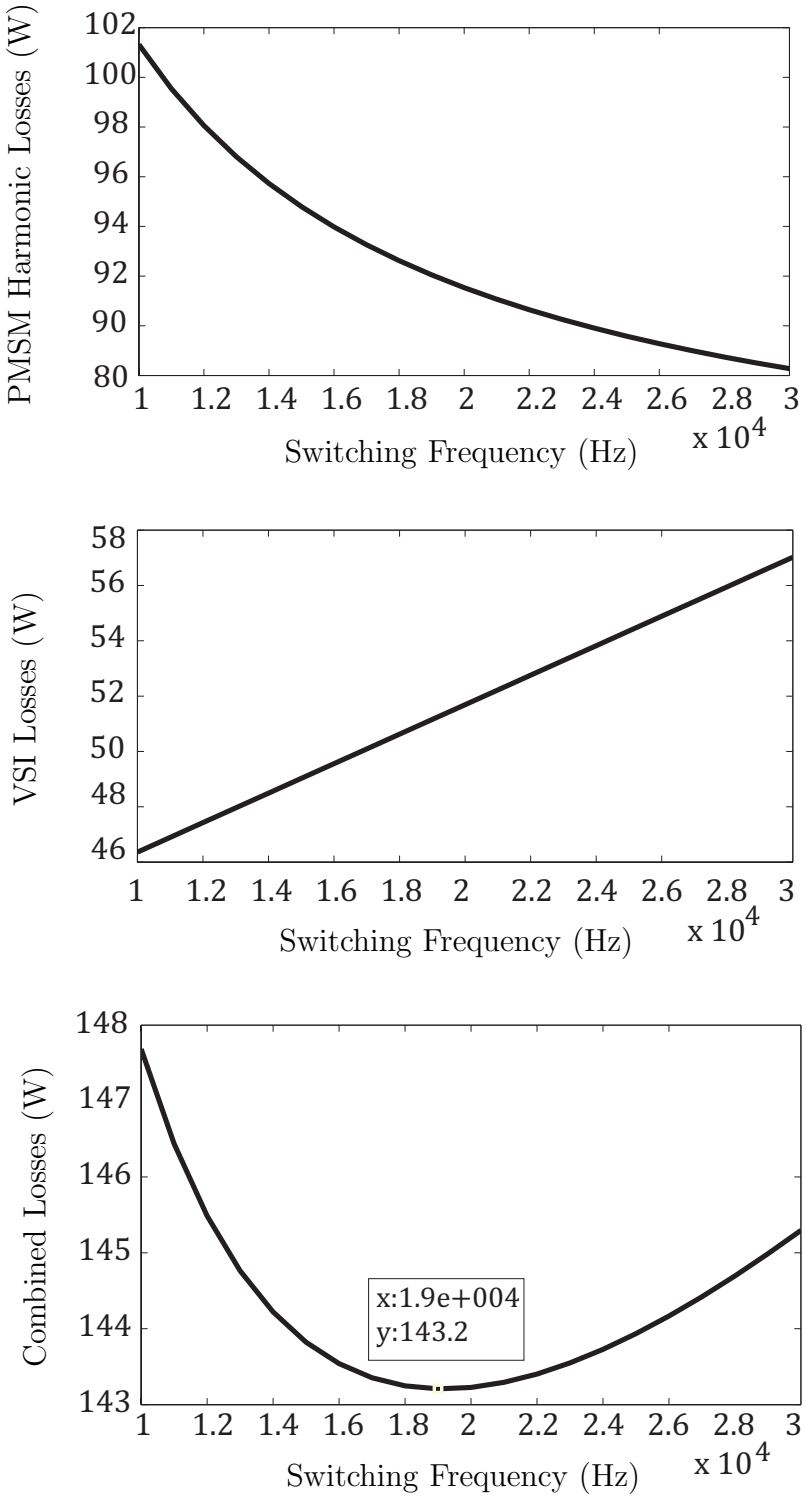

Figure 7.5: Harmonic losses of PMSM, VSI losses and the combined harmonic losses of PMSM and VSI versus switching frequency at rated speed.

in Figure 7.5. The results show that the PMSM harmonics loss decreases as the switching frequency increases. This result is expected since the harmonics content of the stator current

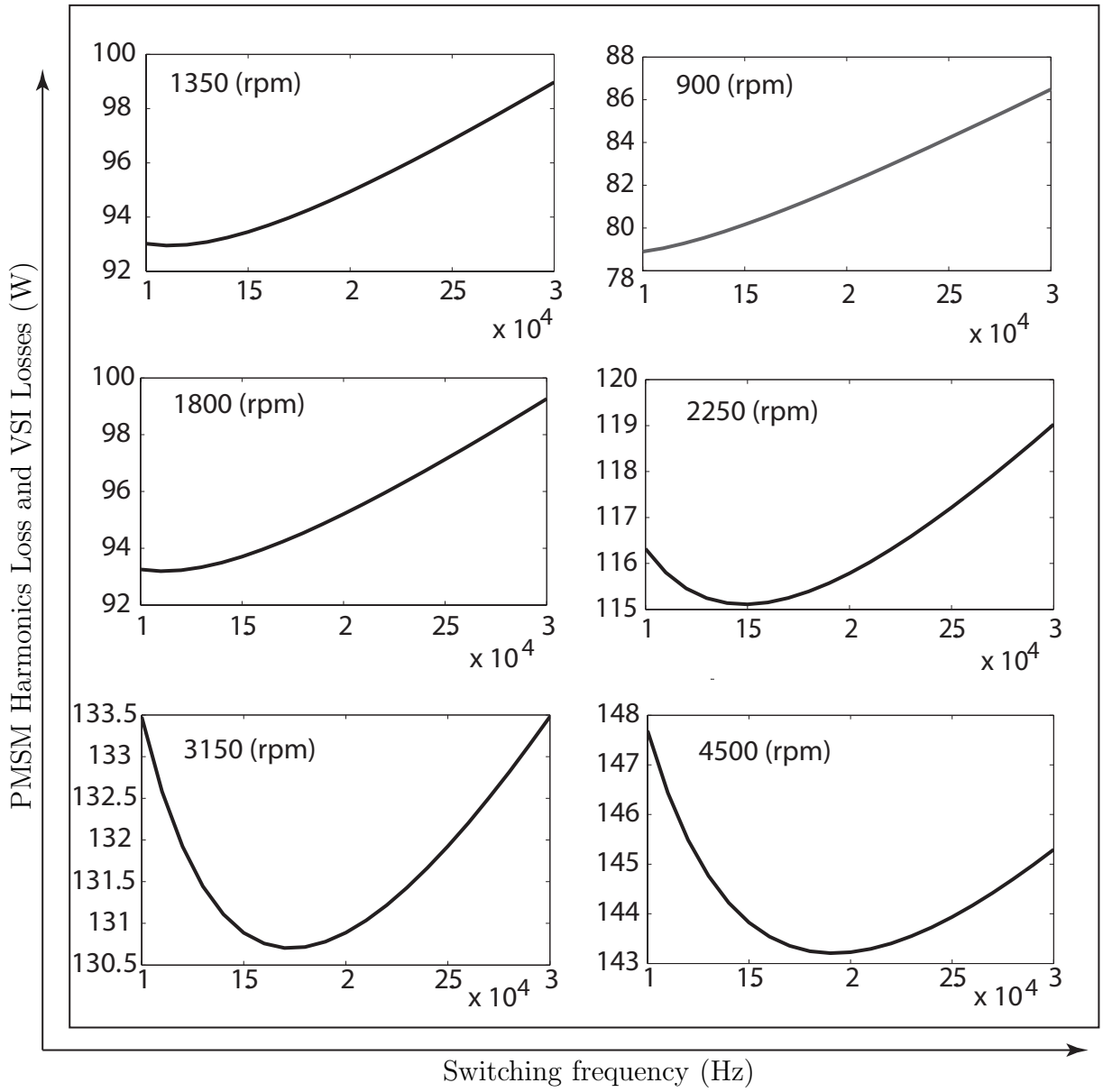

Figure 7.6: Total losses of PMSM harmonics loss and VSI losses versus switching frequency at different speeds.

decreases as the switching frequency increases. Nevertheless, the VSI losses increase as the switching frequency increase. The summation of the above two losses show that the curve is

convex and has global minimum loss value at the switching frequency of 19 kHz. However the specific optimal switching frequency will depend on particular set of design parameters of the VSI. In other words, when the parameters of the VSI such that the loss of VSI higher than the motor harmonics loss at the same range of switching frequency, the curve will be no more convex and almost will be linear.

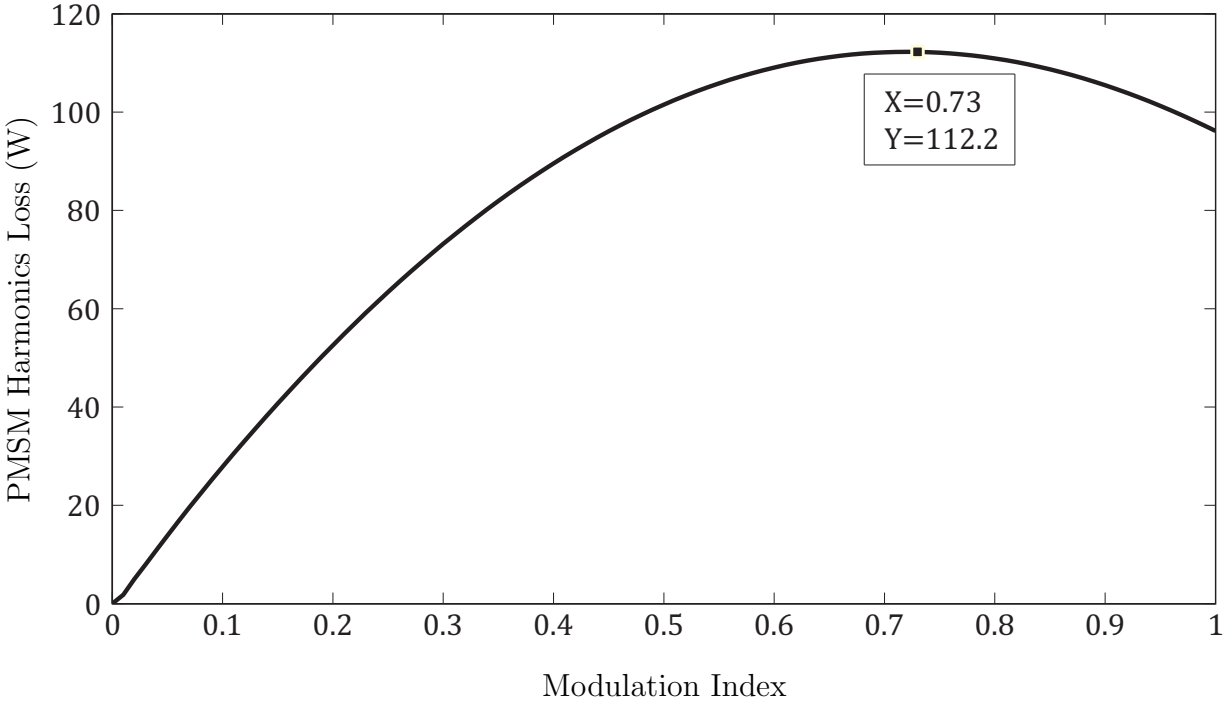

Figure 7.7: PMSM harmonics loss versus modulation index.

Figure 7.6 shows the combined loss of motor harmonics loss and VSI loss versus switching frequency at different speeds and rated torque. The result shows that the total losses increase as the motor speed increases. Also, at low speeds up to 50 % of the rated speed the VSI loss is dominant. When the speed increases, the motor harmonic losses become dominant such that the loss curve becomes convex. Figure 7.7 shows the relationship between PMSM harmonic loss and modulation index. It can be seen that up to $M = 0.73$ the harmonics loss increases as the modulation index increases. As the modulation index passes $M = 0.73$, the

harmonics loss begins to decrease to locally minimum loss value at unity modulation index. Because the loss is minimum near unity modulation index, it is suitable to use variable dc link such that the modulation index is kept near the unity at all loads and speeds.

7.4 Conclusions

The main results of the thesis work can be summarized in the following aspects:

- The motor loss that is caused by the fundamental component of phase currents can be minimized by using the maximum efficiency control strategy with the assumption that the core loss resistance and copper loss resistance are constant under all operating conditions.

- The combined motor-inverter fundamental losses are minimized under maximum efficiency control strategy in the region in which $i_d^{r*} < i_d < 0$.

- PMSM harmonics loss can be minimized by increasing the converter switching frequency with the assumption that SPWM inverter is used without any harmonics injection technique.

- For a given range of switching frequencies in which the motor can work with acceptable performance, the choice of minimal switching frequency would minimize the converter loss.

- For a given range of switching frequencies in which the motor can deliver acceptable performance, the choice of the optimum switching frequency that will minimize motor-inverter losses follows the parametric optimization. The optimal loss point is affected

by the system parameters. Hence, changing of the values of VSI parameters would vary the optimal point of motor-inverter losses.

7.5 Recommendations for Future work

In the thesis work it has been assumed that R_c, K_{hm}, and K_{hm} are constants. Practically, the core losses of the machine are not constant due to the variations in the properties of magnetic material. Modeling the core losses at rated condition may yield inaccurate results in variable speed drive machine. The expected future work is taking into account the change in laminations properties due to operating condions while modeling core losses. However, it is planned to verify the harmonic loss model by using real time controller.

BIBLIOGRAPHY

BIBLIOGRAPHY

[1] G. Slemon, "High-efficiency drives using permanent-magnet motors," *IECON Proceedings*, pp. 725–730, 1993.

[2] M. Rahman, "High efficiency permanent magnet synchronous motors," *IEEE IAS Meeting*, pp. 561–564, 1979.

[3] P. Pillay and R. Krishnan, "Application characteristics of pm synchronous and bdcm motor servo drives," *Conf. Record, IEEE IAS Annual Meeting, Atlanta*, pp. 380–390, Oct. 1987.

[4] G. Slemon and X. Liu, "Core losses in permanent magnet motors," *IEEE Transactions on Magnetics*, vol. 26, no. 5, pp. 1653–1656, Sep. 1990.

[5] R. Colby and D. Novotny, "Efficient operation of pm synchronous motors," *IEEE Transactions on Industry Applications*, vol. IA-23, pp. 1048–1054, Nov./Dec. 1987.

[6] T. H. S. Morimoto, Y. Tong, "Loss minimization control of permanent magnet synchronous motor drives," *Transactions on Industry Applications*, vol. 41, no. 5, pp. 511–517, Oct. 1994.

[7] R. Schiferl and T. Lipo, "Core losses in buried magnet permanent magnet synchronous motors," *IEEE Transactions On Energy Conversion*, vol. 4, no. 2, pp. 279–284, June 1989.

[8] T. L. D. N. L. Xu, X. Xu, "Vector control of a synchronous reluctance motor including saturation and iron loss," *IEEE Transactions on Industry Applications*, vol. 27, no. 5, pp. 978–985, Sep./Oct. 1991.

[9] T. G. J. Flecher, B. Williams, "Efficiency aspects of vector control applied to synchronous reluctance motors," *Conference Proceedings, IEEE IAS meeting*, pp. 294–300, 1995.

[10] R. F. F. Fernandez-Bernal, A. Garcia, "Efficient control of reluctance synchronous machines," *IEEE IECON*, pp. 923–928, 1998.

[11] Y. K. K. J. J. Lee and H. Nam, "Loss distribution of three-phase induction motor fed by pulsewidth-modulated inverter," *IEEE Trans.Magn.*, vol. 40, no. 2, pp. 762–765, Mar. 2004.

[12] E. N. Hildebrand and H. Roehrdanz, "Losses in three-phase induction machines fed by pwm converter," *IEEE Trans. Energy Convers.*, vol. 16, no. 3, pp. 228–233, Sep. 2001.

[13] A. J. M. P. J. Leonard, P. Marketos and M. Lu, "Iron losses under pwmexcitation using a dynamic hysteresis model and finite elements," *IEEE Trans. Magn.*, vol. 42, no. 4, pp. 907–910, Apr. 2007.

[14] T. H. Kim and J. Lee, "Comparison of the iron loss of a flux-reversal machine under four different pwm modes," *IEEE Trans. Magn.*, vol. 43, no. 4, pp. 1725–1728, Apr. 2007.

[15] K. S. H. Toda and M. Ishida, "Effect of material properties on motor iron loss in pm brushless dc motor," *IEEE Trans. Magn.*, vol. 41, no. 10, pp. 3937–3939, Oct. 2005.

[16] A. J. M. J. Sagarduy and F. J. Anayi, "Current losses in electrical steels subjected to matrix and classical pwm excitation waveforms," *IEEE Trans. Magn.*, vol. 42, no. 10, pp. 2818–2820, Oct. 2006.

[17] K. Yamazaki and Y. Seto, "Iron loss analysis of interior permanent- magnet synchronous motors-variation of main loss factors due to driving condition," *IEEE Trans. Ind. Appl.*, vol. 42, no. 4, pp. 1045–1052, Jul./Aug. 2006.

[18] T. L. M. A. Boglietti, A. Cavagnino and P. Pillay, "Comparison of lamination iron losses supplied by pwm voltages: Us and european experiences," *in Proc. IEEE Int. Electr. Machines Drives Conf.*, pp. 1431–1436, May 2005.

[19] M. L. A. Boglietti, P. Ferraris and M. Pastorelli, "Change of the iron losses with the switching supply frequency in soft magnetic materials supplied by pwm inverter," *IEEE Trans. Magn.*, vol. 31, no. 6, pp. 4250–4252, Nov. 1995.

[20] M. L. A. Boglietti, P. Ferraris and F. Profumo, "effects of different modulation index on the iron losses in soft magnetic materials supplied by pwm inverter," *IEEE Trans. Magn.*, vol. 29, no. 6, pp. 3234–3236, Nov 1993.

[21] M. P. P. T. Lotten and N. A. Singampalli, "Lamination core loss measurements in machines operating with pwm or non-sinusoidal excitation," *in Proc. Electr. Machines Drives Conf.*, vol. 2, pp. 743–746, Jun. 1-4 2003.

[22] L. M. F. Sixdenier and J. P. Masson, "Introducing dynamic behavior of magnetic materials into a model of a switched reluctance motor drive," *IEEE Trans. Magn.*, vol. 42, no. 3, pp. 398–404, Mar. 2006.

[23] A. Ruderman, "Electrical machine pwm loss evaluation basics," *in Energy Efficiency in Motor Driven Systems, Heidelberg, Germany*, Sep., 5-8 2005.

[24] M. K. Jamil and N. A. Demerdash, "Harmonics and core losses of permanent magnet dc motors controlled by chopper circuits," *IEEE Trans. Energy Convers.*, vol. 5, no. 2, pp. 408–414, Jun. 1990.

[25] M. K. Jamil and N. Demerdash, "Effects of chopper control circuits on core losses of permanent magnet dc motors," *IEEE Trans. Magn.*, vol. 25, no. 5, pp. 3572–3574, Sep 1989.

[26] M. L. A. Boglietti, P. Ferraris and M. Pastorelli, "About the possibility of defining a standard method for iron loss measurement in soft magnetic materials with inverter supply," *IEEE Trans. Ind. Appl.*, vol. 33, no. 5, pp. 1283–1288, Sep 1997.

[27] C. G. D. Ruifang Liu, Mi, "Modeling of eddy-current loss of electrical machines and transformers operated by pulsewidth-modulated inverters," *IEEE Transactions on Magnetics*, vol. 44, no. 8, pp. 2021–2028, Aug. 2008.

[28] R. Krishnan, "Permanent magnet synchronous and brushless dc motor drives," *Taylor and Francis Group, LLC*, 2010.

[29] H. D. Zhu, Z.Q., "Instantaneous magnetic field distribution in brushless permanent magnet dc motors. ii. armature-reaction field," *IEEE Transactions on Magnetics*, vol. 29, no. 1, pp. 136–142, Jan. 1993.

[30] B. Holmes, D.G.; McGrath, "Opportunities for harmonic cancellation with carrier based pwm for two-level and multi-level cascaded inverters," *Industry Applications Conference,*

1999. Thirty-Fourth IAS Annual Meeting. Conference Record of the 1999 IEEE, vol. 2, pp. 781–788, 1999.

[31] M. Bierhoff and F. Fuchs, "Semiconductor losses in voltage source and current source igbt converters based on analytical derivation," *in Proc. Power Electronics Specialists conference (PESC 04)*, vol. 4, pp. 2836–2842, 2004.

[32] U. Nicolai, T. Reimann, J. Petzoldt, and J. Lutz, "Semikron,applikationshandbuch igbt- und mosfet-leistungsmodule," *ISLE*, 1998.

[33] F. Casanellas, "Losses in pwm inverters using igbts," *IEE Proc. Electr. Power Appl.*, vol. 141, no. 5, pp. 235–239, Sep. 1994.

[34] L. Mestha and P. Evans, "Analysis of on-state losses in pwm inverters," *IEE Proceedings*, vol. 136, no. 4, July 1989.

[35] D. Chung and S. Sul, "Minimum-loss pwm strategy for 3-phase pwm rectifier," *PESC*, vol. 2, pp. 1020–1027, 1997.

[36] K. Zhou and D. Wang, "Relationship between space-vector modulation and three-phase carrier-based pwm: A comprehensive analysis," *IEEE Trans. on Ind. Electr.*, vol. 49, no. 1, pp. 186–196, February 2002.

[37] K. R. PILLAY, P., "Modeling of permanent magnet motor drives," *IEEE TRAN. on Industrial Electronics*, vol. 35, no. 4, Nov. 1988.

[38] T. Instruments, "Field orientated control of 3-phase ac-motors," *Texas Instruments Europe, Literature Number: BPRA073*, Feb. 1998.

[39] S. T. Pekarek, S., "Acsl/graphic modeller component models for electric power education," *IEEE Tran. on Education*, vol. 41, no. 4, Nov. 1998.

[40] U. M. R. P. Moham, N., "Power electronics converters applications and design," *John Wiley and Sons, INC., second edition*, 1995.

[41] T. Y. T. Y. H. T. Morimoto, S., "Loss minimization control of permanent magnet synchronous motor drives," *IEEE TRAN. on industrial Electronics*, vol. 41, no. 5, pp. 511–517, Oct 1994.